

The influence of the secular perturbation of an intermediate-mass companion: I. Eccentricity excitation of disk stars at the Galactic center

XIAOCHEN ZHENG (郑晓晨)¹, DOUGLAS N. C. LIN (林潮)^{2,3} AND SHUDE MAO (毛淑德)^{1,4}

¹*Department of Astronomy, Tsinghua University, Beijing, China*

²*Department of Astronomy and Astrophysics, University of California, Santa Cruz, USA*

³*Institute for Advanced Studies, Tsinghua University, Beijing, China*

⁴*National Astronomical Observatories of China, Chinese Academy of Sciences, 20A Datun Road, Beijing, China*

(Received; Revised; Accepted)

Submitted to ApJ

ABSTRACT

There is a dense group of OB and Wolf-Rayet stars within a fraction of a parsec from the super-massive black hole (SMBH) at the Galactic Center. These stars appear to be coeval and relatively massive. A subgroup of these stars orbits on the same plane. If they emerged with low to modest eccentricity orbits from a common gaseous disk around the central super-massive black hole, their inferred lifespan would not be sufficiently long to account for the excitation of their high orbital eccentricity through dynamical relaxation. Here we analyze the secular perturbation on Galactic Center stars by an intermediate-mass companion (IMC) as a potential mechanism to account for these young disk stars' high eccentricity. This IMC may be either an intermediate-mass black hole (IMBH) or a compact cluster such as IRS-13E. If its orbital angular momentum vector is anti-parallel to that of the disk stars, this perturbation would be effective in exciting the eccentricity of stars with orbital precession rates which resonate with IMC's precession rate. If it orbits around the SMBH in the same direction as the disk stars, the eccentricity of the young stars can still be highly excited by the IMC during the depletion of their natal disk, possible associated with the launch of the Fermi bubble. In this scenario, IMC's precession rate decreases and its secular resonance sweeps through the proximity of the young stars. We carry out numerical simulations with various inclination angles between the orbits of IMC and the disk stars and show this secular interaction is a robust mechanism to excite the eccentricity and inclination of some disk stars.

Keywords: methods: numerical — stars: distances — stars: early-type — stars: kinematics and dynamics — (stars:) planetary systems — stars: solar-type — Galaxy: center — Galaxy: disk

1. INTRODUCTION

It is widely accepted that the Galactic center (GC) of the Milky Way nests a super-massive black hole (SMBH) with a mass $M_{\text{SMBH}} \sim 4 \times 10^6 M_{\odot}$ centered around the Sagittarius A* (Sgr A*) (Ghez et al. 1998, 2003a, 2008; Genzel et al. 1997, 2010; Gillessen et al. 2009; Schödel et al. 2009; Boehle et al. 2016). Within 1 pc³ from the Sgr A*, there are $\sim 10^7$ mostly mature stars (Do et al. 2009; Genzel et al. 2010) as well as a rich and conspicuous population (~ 80) of very young massive and Wolf-Rayet stars with estimated ages of 4 – 6 Myr inside the central $\lesssim 0.5$ pc (Ghez et al. 2003b). At least half of these stars are orbiting around the central

SMBH in a relatively flat clockwise disk. These stars are dubbed as clockwise stars (CWSs) (Löckmann & Baumgardt 2009). The possibility of other stars in an inclined counter-clockwise disk has also been suggested (Paumard et al. 2006) albeit the existence of the second disk remains controversial (Lu et al. 2006, 2009).

It is possible for some mature GC stars to have originated from some stellar clusters which underwent orbital decay from a few kpc away to their present location within the Hubble time (Tremaine 1976; Gerhard 2001; Just et al. 2011). But, the brief (a few Myr) lifespan of the massive main-sequence stars, including the CWSs, casts a strong limit on the distance over which they may have migrated (Portegies Zwart et al. 2002;

Gürkan & Rasio 2005; Madigan et al. 2014). It has been suggested that these stars may be formed in a gaseous disk around the SMBH (Goodman 2003; Levin & Beloborodov 2003). They may also have been rejuvenated from old low-mass stars which are trapped and fed by a disk (Artymowicz et al. 1993). Although there is no evidence of this disk today, its past presence may be inferred from its subsequent depletion, which may be attributed to the outflow from this region in the form of the Fermi bubble (Su et al. 2010). These scenarios are compatible with some CWSs' orbits but not necessarily with all the young stars. The main outstanding issue for the CWSs is that several of them also have large eccentricities (~ 0.7) (Lu et al. 2006; Paumard et al. 2006; Gillessen et al. 2009; Do et al. 2013). If these stars acquired their masses on low or modest eccentricity ($\lesssim 0.5$) orbits in their natal disk (Nayakshin et al. 2007), the time (a few Myr) lapsed since their emergence would not be adequate for local dynamical relaxation processes to excite such large eccentricities (Freitag et al. 2006; Alexander et al. 2007; Madigan et al. 2011). It is possible that some, but not all, of these stars may have originated from a tidally disrupted young cluster (Gerhard 2001; Kim & Morris 2003; Genzel et al. 2003; Maillard et al. 2004; Levin et al. 2005). It is also possible that the CWSs' orbits may be perturbed by a compact companion (Hansen & Milosavljević 2003), a stellar cluster (Schödel et al. 2005) or a second disk (Paumard et al. 2006; Löckmann & Baumgardt 2009).

There are other attempts to explain the orbital properties of these CWSs. In the work of Naoz et al. (2018), they investigated the critical role of stellar binaries in the GC and found that the existence of binaries could significantly vary the inferred stars' orbital properties. According to their discussion, the eccentricities of these disk stars in the GC may be less than those inferred from the kinematic measurement at first glance. In addition, an eccentric nuclear disk could drive new secular instability on stellar orbits in the GC, and amplify deviations of individual orbital eccentricities from the average value (Madigan et al. 2009, 2018). Most recently, Generozov & Madigan (2020) proposed a binary disruption scenario that the S-stars at a distance of 0.01 pc to the GC are the remnants of tidally disrupted binaries from the CWS population. Based on this scenario, they can reproduce the observed S-star semi-major axis and thermal eccentricity distribution.

In this paper, we mainly adopt the perturbation hypothesis with the consideration of an additional effect which may account the rapid excitation of high eccentricity for stars recently formed in a disk with nearly circular orbits. There are several observations that impose

constraints on the mass and separation of any companion to Sgr A*. For example, the proper motion measurement of Sgr A* against background extragalactic source places an upper mass limit of $\sim 10^4 M_\odot$ on any companion within $10^3 - 10^5$ AU around the SMBH (Reid & Brunthaler 2004). The coincidences of the density as well as the kinematic centers of the young stars with the position of the Sgr A* have also been used to limit the companion's mass to be $\lesssim 10^{-2} M_{\text{SMBH}}$ and separation in the range of 0.01 – 1 pc (Yu & Tremaine 2003).

We speculate and assume the culprit to be an infrared-radiation source IRS 13E complex (Krabbe et al. 1995) which contains some massive and early-type stars. Most of these stars appear to be physically bound to the IRS 13E complex (Maillard et al. 2004) which is located at a projected separation of ~ 0.13 pc from the Sgr A*. Recent ALMA observations also unveiled ionized gas which appears flowing along eccentric Keplerian streams around a point-mass potential at the location of IRS 13E (Tsuboi et al. 2017). However, this interpretation would break down if the gas properties of IRS 13E is due to a colliding winds (Wang et al. 2020; Zhu et al. 2020). Although the suggestion that it may be an intermediate-mass black hole (IMBH) remains a controversial issue (Maillard et al. 2004; Hansen & Milosavljević 2003; Kim et al. 2004), its total inferred mass ($\sim 10^4 M_\odot$) would be reasonable if the young stars in the IRS 13E complex are gravitationally bound (Schödel et al. 2005; Tsuboi et al. 2017). This estimated total mass is a few times larger than that from all the massive stars in the region.

The estimated total mass of IRS 13E and its separation from Sgr A* are within the allowable parameter space inferred from the observed properties (Yu & Tremaine 2003; Reid & Brunthaler 2004; Naoz et al. 2020). Moreover, the proper motion of IRS 13E, relative to Sgr A*, seems to be in the same direction as that of stars with counter-clockwise orbits, but opposite to that of CWSs (Genzel et al. 2003), though large uncertainties remain due to the lack of radial velocities and relative distances between it and Sgr A*.

Under these circumstances, the dynamical properties of young stars near Sgr A*, especially in the central parsec, are likely to be significantly affected by the secular perturbation from such a massive companion. Here, we suggest the influence of this intermediate-mass companion (IMC) is particularly strong near its secular resonance where its precession frequency matches that of the stars around Sgr A* induced by it. At the location of its secular resonance, angular momentum is extracted from the stars by the IMC such that their eccentricities are largely excited. During the depletion of the CWSs' natal disk, the location of secular resonance sweeps to-

wards Sgr A^{*} over an extended region, inducing high eccentricity for a large fraction of CWSs. This effect is analogous to that induced by Jupiter on the asteroids in the solar system (e.g., Zheng et al. 2017a,b). Since secular perturbation is imposed over a large distance and accumulates over many orbital periods, this IMC does not need to be an IMBH. A compact and bound stellar cluster with a mass $\sim 10^4 M_\odot$ is adequate to provide sufficient secular perturbation.

In this paper, we consider various contributions to the gravitational potential including that from the supermassive black hole (SMBH), intermediate-mass companion (IMC), the Galactic bulge, disk, and halo as well as that from a gaseous disk out of which the disk stars emerge (§2). In order to analyze the effects of secular interaction, we recapitulate a set of equations analogous to the Laplace planetary equations in celestial mechanics (§3). We utilize these equations to analyze the precession due to various components of the gravitational field and the potential for eccentricity excitation by IRS 13E with various possible orbital configurations. Our analytic calculation is verified by a series of numerical-simulation models of secular resonances in §4. Finally in §5, we summarize our results and discuss their implications.

2. CONTRIBUTING POTENTIALS

Our objective is to investigate the statistically orbital distribution (mainly the semi-major axis a and eccentricity e of their orbits around Sgr A^{*}) of CWSs under the influence of the sweeping secular resonance of an IMC (i.e., IRC 13E, which may be an IMBH or a very compact stellar cluster).

2.1. Numerical method

To solve the Newtonian equation of motion, we adopt the open-source N -body code REBOUND (Rein & Liu 2012), and choose the built-in MERCURIUS integrator (Rein et al. 2019). In this code, a merger can occur if the radius of two objects overlaps. There are several contributors to the potential (Gnedin et al. 2005; Widrow & Dubinski 2005; Kenyon et al. 2008): the central SMBH (Φ_{SMBH}), a satellite IMC (Φ_{IMC}), the Galactic bulge (Φ_{bulge}), the contribution from the potential of the Galactic disk and the halo can be negligible in the central parsec. Within 1 pc from Sgr A^{*}, the SMBH and IMC have Schwarzschild radii (see Table 1), with $s = 2GM/c^2$, where c is the speed of light. For the SMBH's potential, we include the post Newtonian corrections. In order to consider the possibility of the IMC being a dense cluster instead of a point mass IMBH, we also adopt, for one model, a Plummer softening parameter s'_{IMC} for the satellite perturber. For different

components of the Galactic potential, we adopt the conventional prescription:

$$\begin{aligned}\Phi_{\text{SMBH}} &= -\frac{GM_{\text{SMBH}}}{r} + \text{post Newtonian terms}, \\ \Phi_{\text{IMC}} &= -\frac{GM_{\text{IMC}}}{\sqrt{|\vec{r} - \vec{r}_{\text{IMC}}|^2 + s_{\text{IMC}}'^2}}, \\ \Phi_{\text{bulge}} &= -\frac{GM_{\text{bulge}}}{r + a_{\text{bulge}}},\end{aligned}\tag{1}$$

where r is the spherical radius, r_{IMC} is the distance of the IMC from the GC, a_{bulge} is the scaling lengths for the bulge, M_{SMBH} and M_{IMC} are the mass of the SMBH and IMC, M_{bulge} is the mass scaling factor for the bulge (Hernquist 1990). We adopt related parameters from Gnedin et al. (2005). We assume spherical symmetry for the Galactic bulge. Although tri-axial mass distribution in these components can lead to precessions with long term implications on the secular evolution of single and binary stars' orbits (Petrovich & Antonini 2017; Bub & Petrovich 2020), these effects may be negligible in comparison with the IMC's secular perturbation. We introduce a set of mass and length scaling by factors of 4×10^6 and 10^3 respectively (see Table 1) to highlight the similarity between the Galactic center and the Solar system.

In this paper, we focus our attention on the excitation of disk stars within 0.5 pc. Gravity due to the Galactic disk and halo has negligible influence on the dynamical evolution of these stars and the IMC. In paper II of this series, we show that the Galactic disk and halo potentials can significantly modify the trajectories of the unbound hyper-velocity stars at large distances ($> \text{kpc}$) from the Galactic center.

The gravitational potential of a hypothetical geometrically thin gaseous disk (in which the young stars emerge) is determined by its poorly constrained surface density (Σ) distribution. We adopt a prescription similar to our previous models of protostellar disks (Nagasawa et al. 2005; Zheng et al. 2017a). For illustrative purpose, we assume a power-law surface density (Σ) distribution constructed for the minimum mass solar nebula (Hayashi et al. 1985) such that

$$\Sigma = \Sigma_0 \left(\frac{r}{R_0} \right)^{-3/2} e^{-t/\tau_{\text{dep}}} \text{ g/cm}^2, \tag{2}$$

where τ_{dep} is the depletion timescale of the gas nebula, R_0 is a fiducial cylindrical radius. We take into account the possibility that the IMC can strongly perturb the structure of the disk near its orbit analogous to proto giant planets in protostellar disks. But the much less massive young stars have negligible effects on the disk structure, analogous to planetesimals in a protostellar

Table 1. Scaling Galaxy to planetary system

	Observation	Scaling factors	Simulation
M_{bulge}	$1 \times 10^{10} M_{\odot}$	4×10^6	$2.5 \times 10^3 M_{\odot}$
a_{bulge}	0.6 kpc	1×10^3	$1.2 \times 10^5 \text{ AU}$
M_{SMBH}	$4 \times 10^6 M_{\odot}$	4×10^6	$1 M_{\odot}$
s_{SMBH}	$8 \times 10^{-2} \text{ AU}$	1×10^3	$8 \times 10^{-5} \text{ AU}$
τ_{dep}	1.58 – 6.32 Myr	15.8	0.1 – 0.4 Myr
Σ_0	600 – 800 g/cm ²	4	150 – 200 g/cm ²
R_0	1000 AU	1×10^3	1 AU
H/R	0.01	1	0.01
M_{IMC}	$1 \times 10^4 M_{\odot}$	4×10^6	$2.5 M_J$
s_{IMC}	$3 \times 10^4 \text{ km}$	1×10^3	30 km
s'_{IMC}	5000 AU	1×10^3	5 AU
a_{IMC}	0.3 – 0.4 pc	1×10^3	60 – 80 AU
e_{IMC}	0.2 – 0.4	1	0.2 – 0.4
m_{\star}	$12 M_{\odot}$	4×10^6	$1 M_{\oplus}$
s_{\star}	$1.5 \times 10^6 \text{ km}$	1×10^3	$1.5 \times 10^3 \text{ km}$
a_{\star}	0.05 – 0.5 pc	1×10^3	10 – 100 AU
v_{\star}	$\sim 200 - 600 \text{ km/s}$	63	$\sim 0.1 - 0.3 v_{\oplus}$

NOTE— $M_{\text{SMBH}}, M_{\text{bulge}}$ are the masses of SMBH, Galactic bulge; a_{bulge} is the characteristic length scales of the Galactic bulge; $M_{\text{IMC}}, a_{\text{IMC}}, e_{\text{IMC}}$ are the mass, semi-major axis and eccentricity of the intermediate mass companion (IMC, which is either an IMBH or stellar cluster); $s_{\text{SMBH}}, s_{\text{IMC}}$ are the Schwarzschild radii of the SMBH and IMC; s'_{IMC} is the softening parameter to represent IRS 13E as a stellar cluster, $\Sigma_0, H/R, \tau_{\text{dep}}$ are the reference surface density, aspect ratio, characteristic depletion time of the gaseous disk, $m_{\star}, s_{\star}, a_{\star}, v_{\star}$ are the mass, radius, initial semi-major axis, and velocity of the stars.

disk. For models in which the IMC's orbital angular momentum vector is parallel to that of the disk (co-orbiting models), we assume the presence of a gap around its orbit at

$$a_{\text{in/out}} = a_{\text{IMC}}(1 \mp e_{\text{IMC}}) \left[1 \mp \left(\frac{M_{\text{IMC}}}{3M_{\text{SMBH}}} \right)^{1/3} \right], \quad (3)$$

where a_{IMC} and e_{IMC} are the orbital parameters of the IMC. The structure of this gap can modify the disk's force on the IMC and precession rate of its orbit (Ward 1981; Nagasawa et al. 2005; Zheng et al. 2017a) such

that

$$f_{\text{gap,gas}} = 2\pi G \Sigma \sum_{l=0}^{\infty} \left[\frac{(2l)!}{2^{2l}(l!)^2} \right]^2 \left(\frac{2}{4l+1} \right) \times \left[(2l) \left(\frac{r}{a_{\text{out}}} \right)^{2l+1/2} - (2l+1) \left(\frac{a_{\text{in}}}{r} \right)^{2l+1/2} \right]. \quad (4)$$

For the case where we consider the possibility that the IMC's orbital angular momentum vector is anti-parallel to that of the disk (counter-orbiting models), the IMC does not open up a gap in the gaseous disk. We also assume the embedded stars do not have sufficient mass to open gaps near their orbit and their apsidal precession induced by the gas disk is dominated by the gas in their neighborhood. The disk's gravitational force on them can be computed as

$$f_{\text{emb,gas}} = -4\pi G \Sigma Z_k, \quad (5)$$

where $Z_k = 1.094$ is the same as in Ward (1981); Nagasawa et al. (2005); Zheng et al. (2017a).

In addition, a post-Newtonian correction for the central SMBH is included, using the relativity formula from Kidder (1995); Nagasawa et al. (2005), in the form as

$$\vec{f}_{\text{rela}} = \frac{GM_{\text{tot}}}{r^2 c^2} \left\{ 2(2-\mu)v_r \vec{v} - \left[(1+3\mu)v^2 - 2(2+\mu) \frac{GM_{\text{tot}}}{r} - \frac{3}{2}\mu v_r^2 \right] \frac{\vec{r}}{r} \right\}, \quad (6)$$

where v_r is the velocity in the r direction, and $M_{\text{tot}} = M_{\text{SMBH}} + m$, $\mu = mM_{\text{SMBH}}/M_{\text{tot}}^2$. Note that it is just a simple 1-post-Newtonian form. Motivated by the work of Rodriguez et al. (2018), we have made a further test on the 2-post-Newtonian term. We find that the higher-order correction makes negligible correction on most residual orbits, except for those highly eccentric orbits, which have the closest distance to the central SMBH smaller than $\sim 10^{-5} \text{ pc}$. Therefore, our assumption concerning general relativity is appropriate in this work. In the second paper of this series, we extend this formula to include the higher-order term (Kidder 1995) to avoid considerable energy alterations during close encounters with the SMBH.

2.2. Numerical models

In order to investigate the effects of sweeping secular resonance on the evolution of GC stars and its parameter dependence, we test a series of numerical models with various setups. Table 2 lists all these models, including simulations with three different gas-disk depletion timescales. In all cases, the stars are assumed to reside

Table 2. Parameters for various numerical simulations

models	$s'_{\text{IMC}}(\text{AU})^a$	$i_{\text{IMC},*}(^{\circ})^b$	$i_{*}(^{\circ})^c$	Gas Disk Potential ^d	Gas Disk Gap ^e
NGD	0	0	0	—	—
fiducial	0	0	0	+	+
SOFT	5000	0	0	+	+
CCW	0	180	0	+	—
CCW-NGD	0	180	0	—	—
I30	0	30	0	+	—
I30-NGD	0	30	0	—	—
I60	0	60	0	+	—
I60-NGD	0	60	0	—	—
I60-IS60	0	60	60	+	—
I60-IS60-NGD	0	60	60	—	—

NOTE— ^a The softening parameter of IMC's potential. ^b The initial mutual inclination between the orbits of IMC and disk stars. ^c The initial inclination of the orbit of disk stars (gas disk) relative to the Galactic disk (reference plane). ^d The presence of the gas disk potential. ^e The presence of a gas-free gap around the IMC's orbit.

in the gaseous disk with circular orbits initially. In the proximity of the SMBH, the potential contribution from the Galactic disk is negligible. For simplicity, we consider the case that the disk stars' initial orbits are in the same plane as that of the Galactic disk. Contributions from the Galactic disk and halo are important for the hypervelocity stars after they are ejected from the proximity of the SMBH. An inclination angle between the disk stars' orbits and the Galactic disk may introduce some modification to the asymptotic kinematic properties of the HVSs, we will discuss this circumstance in paper II of this series.

We highlight the influence of the sweeping secular resonance by turning off gravity due to the gas in a comparative model NGD. In all but one model, the companion's potential is assumed to be that of a point mass IMBH. Since the IMBH nature of IRS 13E continues to be a controversial issue, we also consider the possibility of the IMC being a dense star cluster with a Plummer-type mass distribution in the SOFT model with a non-zero s'_{IMC} (see Table 2).

In the fiducial, NGD, and SOFT models, we assume the Sgr A*, companion, stars and gaseous disk are all in the same plane, and their orbital angular momentum vectors are aligned. In the CCW model, we consider the possibility that the IMC's orbit is anti-parallel to that of the stars and gaseous disks, as suggested by some observations of IRS 13E (Genzel et al. 2003). In this paper, we present the analysis and simulations of these co-planar models. We also consider a series of 3-d cases with various misalignment angles between the IMC's and the

stars' initial orbital planes. For those simulations, we approximate the gaseous disk's force in the radial direction of the gaseous disk with $f_{\text{emb,gas}}(R_{\text{IMC}})$ (Equation (5)) in models I30 and I60 to take into account the possible absence of a gap at the gaseous disk radial location R_{IMC} . For both models, the force in the (z , the distance above the disk) direction normal to the gaseous disk plane is approximated with

$$f_{z,\text{gas}} = -2\pi G\Sigma(R) \frac{\text{sign}(z)(z/H)^2}{1 + (z/H)^2}. \quad (7)$$

The gaseous disk's aspect ratio H/R is assumed to be 0.01 (see Table 1) at R_0 , with the form $H/R = (H_0/R_0)(R/R_0)^{1/4}$. The gravitational stability parameter of the disk is

$$Q = \frac{c_s\Omega}{\pi G\Sigma} = \frac{H_0}{R_0} \frac{M_{\text{SMBH}}}{\pi\Sigma_0 R_0^2} \left(\frac{R}{R_0}\right)^{-1/4} \sim \text{a few } 10, \quad (8)$$

such that the effects of self gravity is negligible in these models. For comparison, we also examine the cases without the gaseous disk.

3. CELESTIAL MECHANICS OF A REPRESENTATIVE STAR

In the numerical simulations, we integrate the stars' orbits based on the Newtonian equation of motion. In the analysis of this process, it is useful to adopt Laplace's approach in celestial mechanics by averaging periodic velocity and position changes over an orbital timescale. We consider the secular (long-term) evolution of orbital elements, including their semi-major axis a , eccentricity e , inclination i , longitudes of the periastron ϖ , and

ascending node Ω . This approach provides physical insights into the dominant contribution of various effects.

3.1. Secular interaction between IMC and the disk stars

For stars reside within the inner parsec from the Sgr A*, the predominant contributor to the gravitational is Φ_{SMBH} and other components can be treated as perturbations. This configuration is closely analogous to solar system dynamics, where the secular evolution in celestial mechanics can be approximated by planetary equations (Murray & Dermott 2000). We first construct a set of disturbing function

$$\mathfrak{R} = \mathfrak{R}^{(\text{sec})} + \mathfrak{R}^{(\text{bulge})} + \mathfrak{R}^{(\text{gas})} + \mathfrak{R}^{(\text{GR})}. \quad (9)$$

In addition, general relativity (GR) is only significant in the limit of small periastron distance, $r_p = a(1 - e)$, see also in Figure 2. For most of disk stars and the IMC at distance $\sim 0.05 - 0.5$ pc, we neglect the GR precession in our analytic approximation.

The secular perturbation between the disk star and the IMC can be expressed as

$$\begin{aligned} \mathfrak{R}_\star^{(\text{sec})} &= GM_{\text{IMC}} \left(\frac{1}{|\vec{r}_{\text{IMC}} - \vec{r}_\star|} - \frac{\vec{r}_\star \cdot \vec{r}_{\text{IMC}}}{r_{\text{IMC}}^3} \right), \\ \mathfrak{R}_{\text{IMC}}^{(\text{sec})} &= Gm_\star \left(\frac{1}{|\vec{r}_\star - \vec{r}_{\text{IMC}}|} - \frac{\vec{r}_\star \cdot \vec{r}_{\text{IMC}}}{r_\star^3} \right). \end{aligned} \quad (10)$$

Since $m_\star \ll M_{\text{IMC}}$, the secular perturbation of disk stars on the IMC, $\mathfrak{R}_{\text{IMC}}^{(\text{sec})}$, can be ignored.

When we average over an orbit, only the perturbation function's secular term does not contain mean longitude remain. We adopt the second-order expansion of the direct part of the disturbing function following Equation (7.8 – 7.12) in the Murray & Dermott (2000), as

$$\begin{aligned} \mathfrak{R}_\star^{(\text{sec})} &= n_\star a_\star^2 \left[\frac{1}{2} A_1 e_\star^2 + A_2 e_\star e_{\text{IMC}} \cos(\varpi_\star - \varpi_{\text{IMC}}) \right. \\ &\quad - 2A_1 \sin^2\left(\frac{i_\star}{2}\right) + 4A_1 \sin\left(\frac{i_\star}{2}\right) \sin\left(\frac{i_{\text{IMC}}}{2}\right) \\ &\quad \left. \times \cos(\Omega_\star - \Omega_{\text{IMC}}) \right], \\ \text{with } A_1 &= \frac{n_\star \mu_\star \alpha^2}{4} b_{3/2}^{(1)} \text{ and } A_2 = -A_1 \frac{b_{3/2}^{(2)}}{b_{3/2}^{(1)}}, \end{aligned} \quad (11)$$

where $(a_\star, e_\star, i_\star, \varpi_\star, \Omega_\star, n_\star)$ and $(a_{\text{IMC}}, e_{\text{IMC}}, i_{\text{IMC}}, \varpi_{\text{IMC}}, \Omega_{\text{IMC}}, n_{\text{IMC}})$ are the semi-major axis, eccentricity, inclination, longitudes of the peri-astron, ascending node, mean angular velocity of the disk star and the IMC, respectively. We have assumed that $a_\star < a_{\text{IMC}}$ as

most stars are located within the orbit of the IMC. In the limit $m_\star \ll M_{\text{IMC}} \ll M_{\text{SMBH}}$, $n_\star \approx \sqrt{GM_{\text{SMBH}}/a_\star^3}$, $\mu_\star \approx M_{\text{IMC}}/M_{\text{SMBH}}$, $b_{3/2}^{(1)}$ and $b_{3/2}^{(2)}$ are Laplace coefficients for the semi-major axis ratio $\alpha \equiv a_\star/a_{\text{IMC}}$.

The stars' Lagrangian equations of motion are

$$\begin{aligned} \frac{d\varpi_\star^{(\text{sec})}}{dt} &= \left[A_1 + A_2 \left(\frac{e_{\text{IMC}}}{e_\star} \right) \cos(\varpi_\star - \varpi_{\text{IMC}}) \right] \sqrt{1 - e_\star^2} \\ &\quad - 2A_1 \left[\sin^2\left(\frac{i_\star}{2}\right) - \sin\left(\frac{i_\star}{2}\right) \sin\left(\frac{i_{\text{IMC}}}{2}\right) \right. \\ &\quad \left. \times \cos(\Omega_\star - \Omega_{\text{IMC}}) \right] \frac{1}{\sqrt{1 - e_\star^2}}, \\ \frac{de_\star^{(\text{sec})}}{dt} &= A_2 e_{\text{IMC}} \sin(\varpi_\star - \varpi_{\text{IMC}}) \sqrt{1 - e_\star^2}. \end{aligned} \quad (12)$$

In the limit of small e_\star , we approximate $\sqrt{1 - e_\star^2} \simeq 1$. Since the disk stars' secular perturbation on the IMC is negligible

$$\frac{de_{\text{IMC}}^{(\text{sec})}}{dt} \simeq \frac{d\varpi_{\text{IMC}}^{(\text{sec})}}{dt} \simeq 0. \quad (13)$$

3.2. Precession due to the bulge and other components of the Galactic potential

The bulge also induces disk stars and IMC to precess at rates comparable to that of the stars under the IMC's secular perturbation. At locations $r \ll a_{\text{bulge}}$, the disturbing function due to perturbation from the potential of the Galactic bulge can be written as

$$\mathfrak{R}^{(\text{bulge})} = \frac{GM_{\text{bulge}}}{a_{\text{bulge}}} \left(1 - \frac{r}{a_{\text{bulge}}} \right). \quad (14)$$

This disturbing function can be further simplified without the r independent term.

Although the bulge potential is assumed to be spherically symmetric, the stars' eccentricity (relative to the SMBH and is defined by the Kepler's equation) varies along the orbit because the bulge's potential is contributed by a distributed (rather than a point) mass. Nevertheless, after averaging over the stars' orbits, the Lagrange's equations for the orbital elements are reduced to

$$\frac{d\varpi^{(\text{bulge})}}{dt} = -\frac{GM_{\text{bulge}}}{a_{\text{bulge}}^2} \frac{\sqrt{1 - e^2}}{na} \quad (15)$$

and $(de/dt)^{(\text{bulge})} = 0$ because the potential of a spherically symmetric bulge does not induce any net changes in the star's orbital energy and angular momentum on a secular timescale.

Note that the precession rate is relative to the orbits of either the disk stars or the IMC. Since $(d\varpi/dt)^{(\text{bulge})} <$

0, the precession of stars/IMC on a clockwise/counter-clockwise orbit is counter-clock/clockwise. Within 1 pc^3 from the Sgr A*, we neglect contributions to the potential from the Galactic disk and halo because they are much weaker than those due to IMC and the Galactic bulge.

3.3. Precession due to the gaseous-disk's potential

The precession rate of the periastron's longitude induced by the gas disk can be classified as two types according to various situations. Disk stars generally do not have sufficient mass to open a gap in the proximity of their orbit. Unless they are very close to the IMC, their precession rate can be derived from Equation (5) such that

$$\frac{d\varpi}{dt}^{(\text{emb,gas})} \approx -\frac{\pi G \Sigma(a) Z_k}{n a}. \quad (16)$$

If the IMC orbits around the SMBH in the opposite direction as the gaseous disk, it would not be able to open a gap such that its precession rate would have the same magnitude but with an opposite sign.

In contrast, if the IMC revolves around the SMBH in the same direction as the gas disk and the disk stars, it would be able to open a gap (Equation (3)). Under such a circumstance, we can derive its precession rate from Equation (4), such that

$$\begin{aligned} \frac{d\varpi_{\text{IMC}}}{dt}^{(\text{gap,gas})} &\approx \frac{\pi G \Sigma(a_{\text{IMC}})}{n_{\text{IMC}} a_{\text{IMC}}} Z_{\text{IMC}} \quad \text{where} \\ Z_{\text{IMC}} &= \sum_{l=1}^{\infty} \left[\frac{(2l)!}{2^{2l} (l!)^2} \right]^2 \frac{4l(2l+1)}{4l+1} \\ &\times \left[\left(\frac{a_{\text{IMC}}}{a_{\text{out}}} \right)^{2l+1/2} + \left(\frac{a_{\text{in}}}{a_{\text{IMC}}} \right)^{2l+1/2} \right]. \end{aligned} \quad (17)$$

Due to the presence of the gap, IMC's direction of precession is opposite to that of the disk stars (Nagasawa et al. 2005; Ward 1981). Similar to $(d\varpi/dt)^{(\text{bulge})}$, negative value of $(d\varpi/dt)^{(\text{emb,gas})}$ implies the periastron longitude' regression relative to the sense of stars'/IMC's orbit. Here we neglect the effect of eccentricity damping by either tidal or hydrodynamic drag and assume $(da/dt)^{(\text{gas})} = (de/dt)^{(\text{gas})} = 0$.

3.4. Relative longitude of periastron between the disk stars' and co-orbiting or counter-orbiting IMC

The orbital evolution of both the disk stars and IMC can be computed by the sum of all contributions. For simplicity, we only analyze the configuration that the disk stars, the gaseous disk, and the IMC are coplanar. (The non-coplanar models are simulated numerically in

the next section.) There are two limiting co-orbiting and counter-orbiting cases, in which the orbital angular momentum vector of the IMC is either a) parallel or b) anti-parallel with respect to that stars and their natal gaseous disk. Without the loss of generality, we can set $i_{\star} = 0$ so that $i_{\text{IMC}} = 0$ corresponds to the co-orbiting case and $i_{\text{IMC}} = \pi$ to the counter-orbiting case. In both cases, the precession rate of the disk stars is

$$\begin{aligned} \frac{d\varpi_{\star}}{dt} &= \frac{d\varpi_{\star}^{(\text{sec})}}{dt} + \frac{d\varpi_{\star}^{(\text{bulge})}}{dt} + \frac{d\varpi_{\star}^{(\text{emb,gas})}}{dt} \\ &\simeq A_1 + A_2 \left(\frac{e_{\text{IMC}}}{e_{\star}} \right) \cos(\varpi_{\star} - \varpi_{\text{IMC}}) \\ &\quad - \frac{GM_{\text{bulge}}/a_{\text{bulge}}^2}{n_{\star} a_{\star}} - \frac{\pi G \Sigma(a_{\star}) Z_k}{n_{\star} a_{\star}}. \end{aligned} \quad (18)$$

The co-orbiting IMC (with $i_{\text{IMC}} = i_{\star} = 0$) can open a gap in the gaseous disk such that its precession rate becomes

$$\begin{aligned} \frac{d\varpi_{\text{IMC}}}{dt} &= \frac{d\varpi_{\text{IMC}}^{(\text{bulge})}}{dt} + \frac{d\varpi_{\text{IMC}}^{(\text{gap,gas})}}{dt} \\ &\approx -\frac{GM_{\text{bulge}}/a_{\text{bulge}}^2}{n_{\text{IMC}} a_{\text{IMC}}} + \frac{\pi G \Sigma(a_{\text{IMC}}) Z_{\text{IMC}}}{n_{\text{IMC}} a_{\text{IMC}}}, \end{aligned} \quad (19)$$

We obtain, in the limit of small e_{\star} , the evolution of $\xi \equiv e_{\star}/e_{\text{IMC}}$ and the angle between IMC's and the stars' longitude of periastron $\eta = \varpi_{\star} - \varpi_{\text{IMC}}$ from Equations (18) and (19),

$$\begin{aligned} \frac{d\eta}{dt} &\simeq A_{\text{tot}} + \frac{A_2}{\xi} \cos \eta \quad \text{and} \quad \frac{d\xi}{dt} \simeq A_2 \sin \eta, \\ A_{\text{tot}} &= A_1 - \frac{GM_{\text{bulge}}}{a_{\text{bulge}}^2} \left(\frac{1}{n_{\star} a_{\star}} - \frac{1}{n_{\text{IMC}} a_{\text{IMC}}} \right) \\ &\quad - \pi G \left(\frac{\Sigma(a_{\star}) Z_k}{n_{\star} a_{\star}} + \frac{\Sigma(a_{\text{IMC}}) Z_{\text{IMC}}}{n_{\text{IMC}} a_{\text{IMC}}} \right). \end{aligned} \quad (20)$$

In the above expression, we have taken into account the effect of a gap is to induce IMC to precess in the opposite direction as the stars.

Within an order of magnitude,

$$\begin{aligned} \frac{|d\varpi_*/dt^{(\text{bulge})}|}{|d\varpi_*/dt^{(\text{sec})}|} &\simeq \mathcal{O}(4B_1), \\ \frac{|d\varpi_*/dt^{(\text{gas})}|}{|d\varpi_*/dt^{(\text{sec})}|} &\simeq \mathcal{O}\left(\frac{B_2 Z_k}{\alpha^{3/2} \exp(t/\tau_{\text{dep}})}\right), \\ \frac{|d\varpi_{\text{IMC}}/dt^{(\text{bulge})}|}{|d\varpi_*/dt^{(\text{sec})}|} &\simeq \mathcal{O}\left(\frac{4B_1}{\alpha^{1/2}}\right), \\ \frac{|d\varpi_{\text{IMC}}/dt^{(\text{gas})}|}{|d\varpi_*/dt^{(\text{sec})}|} &\simeq \mathcal{O}\left(\frac{B_2 Z_{\text{IMC}}}{\alpha^{1/2} \exp(t/\tau_{\text{dep}})}\right), \end{aligned} \quad (21)$$

$$\text{with } B_1 \equiv \frac{M_{\text{bulge}} a_{\text{IMC}}^2}{M_{\text{IMC}} a_{\text{bulge}}^2}, \quad B_2 \equiv \frac{M_D a_{\text{IMC}}^{1/2}}{M_{\text{IMC}} R_0^{1/2}},$$

where $M_D = 4\pi\Sigma_0 R_0^2$ is the characteristic disk mass. Different components of A_{tot} have similar magnitude at $t = 0$ and the contribution from the gaseous disk decreases with time as it is depleted.

A counter-orbiting IMC (with $i_{\text{IMC}} = \pi$ and $i_* = 0$) cannot open up a gap in the stars' natal gaseous disk. In this case, ϖ_{IMC} and ϖ_* are measured in the opposite sense. In the determination of η for the IMC's secular perturbation on the disk stars, we need bring the values of ϖ_{IMC} to the same frame where ϖ_* is measured by switching its sign such that $\eta = \varpi_* + \varpi_{\text{IMC}}$ and

$$\begin{aligned} \frac{d\eta}{dt} &\simeq A_{\text{tot}} + \frac{A_2}{\xi} \cos \eta \quad \text{and} \quad \frac{d\xi}{dt} \simeq A_2 \sin \eta, \\ A_{\text{tot}} &= A_1 - \frac{GM_{\text{bulge}}}{a_{\text{bulge}}^2} \left(\frac{1}{n_* a_*} + \frac{1}{n_{\text{IMC}} a_{\text{IMC}}} \right) \\ &\quad - \pi G \left(\frac{\Sigma(a_*) Z_k}{n_* a_*} + \frac{\Sigma(a_{\text{IMC}}) Z_k}{n_{\text{IMC}} a_{\text{IMC}}} \right). \end{aligned} \quad (22)$$

3.5. Relative importance of the Galactic bulge, gaseous disk, and IMC's orbit

Equations (20) and (22) are the governing equations for disk stars' eccentricity excitation and nodal precession. The characteristic timescale can be normalized as a dimensionless independent variable

$$\tau = \frac{M_{\text{IMC}}}{M_{\text{SMBH}}} \frac{n_{\text{IMC}} t}{4} \quad (23)$$

$$\frac{d\eta}{d\tau} \simeq A'_{\text{tot}} - \frac{\alpha^{1/2} b_{3/2}^{(2)}}{\xi} \cos \eta, \quad \frac{d\xi}{d\tau} = -\alpha^{1/2} b_{3/2}^{(2)} \sin \eta, \quad (24)$$

$$\begin{aligned} A'_{\text{tot}} &= \alpha^{1/2} b_{3/2}^{(1)} - 4B_1(\alpha^{1/2} \mp 1) \\ &\quad - \frac{B_2}{\exp(t/\tau_{\text{dep}})} \left(\frac{Z_k}{\alpha} + Z_{\text{IMC},k} \right). \end{aligned} \quad (25)$$

The negative/positive signs inside the bracket of the second term on the right hand side of Equation (25) and the IMC and k subscript of Z refer to co-orbiting and counter-orbiting IMC respectively.

The rate and amount of eccentricity excitation of the disk stars (Eq. 24) is determined by the model parameters α , B_1 and B_2 . Based on our adopted model parameters (Table 1), with $\Sigma_0 = 600 \text{ g/cm}^2$,

$$\begin{aligned} B_1 &= 0.25, & B_2 &= 0.66 & \text{for } a_{\text{IMC}} &= 0.3 \text{ pc}, \\ B_1 &= 0.44, & B_2 &= 0.76 & \text{for } a_{\text{IMC}} &= 0.4 \text{ pc}. \end{aligned} \quad (26)$$

The Laplace coefficients $b_{3/2}^{(1)}(\alpha = 0.3) = 1.07$, $b_{3/2}^{(1)}(0.5) = 2.58$, $b_{3/2}^{(2)}(0.3) = 0.4$, and $b_{3/2}^{(2)}(0.5) = 1.56$. And $Z_{\text{IMC}} = 1.3$. With this range of values, the contribution from IMC's secular perturbation, Galactic bulge, and gaseous disk have comparable influence.

3.6. Excitation of disk stars' eccentricity due to IMC and Galactic bulge

For simplicity, we first consider the contribution of the IMC and Galactic bulge and set $\Sigma_0 = 0$ so that $B_2 = 0$. We adopt $a_{\text{IMC}} = 0.3 \text{ pc}$, $e_{\text{IMC}} = 0.2$, and $a_* = 0.15 \text{ pc}$ (i.e. $\alpha = 0.5$) as a typical illustrative example. The magnitude of

$$A'_{\text{tot}} \simeq 2.1 \quad \text{or} \quad A'_{\text{tot}} \simeq 0.1 \quad (27)$$

for co-orbiting and counter-orbiting IMC respectively.

We assume that the disk stars formed with negligible e_* and $\xi = e_*/e_{\text{IMC}} \ll 1$ such that $|A'_{\text{tot}}| \ll |\alpha^{1/2} b_{3/2}^{(2)}/\xi|$. While the IMC precesses at its own pace (determined by $d\varpi_{\text{IMC}}^{(\text{bulge})}/dt$), η evolves to a critical non-zero value

$$\eta_{\text{crit}} = \cos^{-1} \left(\frac{A'_{\text{tot}} \xi}{\alpha^{1/2} b_{3/2}^{(2)}} \right) \quad (28)$$

such that $d\eta/dt \simeq 0$. For $\xi \ll 1$, $\eta_{\text{crit}} \simeq -\pi/2 + \epsilon$ where $0 < \epsilon \ll 1$.

Under this secular resonance (a match between the IMC's and the stellar precession rates), η_{crit} monotonically increases to 0 and e_* (and ξ) increases at slowly-declining rate towards a critical value

$$\xi_{\text{limit}} \simeq \frac{\alpha^{1/2} b_{3/2}^{(2)}}{|A'_{\text{tot}}|} \quad \text{and} \quad e_{*,\text{limit}} = e_{\text{IMC}} \xi_{\text{limit}} \quad (29)$$

on a characteristic timescale

$$\tau_{\text{ecc}} \simeq \frac{4M_{\text{SMBH}}}{n_{\text{IMC}} M_{\text{IMC}} |A'_{\text{tot}}|}. \quad (30)$$

Substitute $\xi_{\star, \text{limit}}$ and τ_{ecc} into Equation (24), we find

$$\tau_{\text{ecc}} \frac{\partial \eta}{\partial t} = 1 - \frac{\xi_{\text{limit}}}{\xi} \cos \eta, \quad \tau_{\text{ecc}} \frac{\partial}{\partial t} \left(\frac{\xi}{\xi_{\text{limit}}} \right) = -\sin \eta. \quad (31)$$

Provided $e_{\star, \text{limit}} < 1$, there is a transition from monotonic eccentricity (e_{\star} and ξ) growth to a state of liberation (with η around 0 and ξ around ξ_{limit}). The liberation period is $\sim \tau_{\text{ecc}}/2\pi$ and the liberation amplitude of ξ is limited to $\sim \xi_{\text{limit}}$. Stars with $\xi \gtrsim 2 \xi_{\text{limit}}$ circulate with limited amplitude in ξ and $(-\pi, \pi)$ in η .

If the IMC revolves around the SMBH in the same direction as the disk stars, $e_{\star, \text{limit}} \sim 0.1$ within $\tau_{\text{ecc}} \sim 1$ Myr. But, if the IMC revolves around the SMBH in the opposite direction as the disk stars, $e_{\star, \text{limit}} (> 1)$ cannot be reached before e_{\star} approaches unity on a timescale

$$\tau_{\text{parabolic}} \simeq \frac{4(M_{\text{SMBH}}/M_{\text{IMC}})}{n_{\text{IMC}} \alpha^{1/2} b_{3/2}^{(2)} e_{\text{IMC}}} \lesssim 10 \text{ Myr}. \quad (32)$$

In this case, the stars' periastron can reach the proximity of the SMBH and be ejected as high velocity stars, although we need to take into account the factor of $\sqrt{1 - e_{\star}^2}$ and relativistic precession in quenching the evolution of both $d\eta/dt$ and $d\xi/dt$ as e_{\star} approaches unity.

3.7. Nature of sweeping secular resonance

We now add the contribution of the gas disk potential (with $\Sigma_0 = 600 \text{ g cm}^{-2}$ as in Eq. 26). The value of A'_{tot} is modified from those in Equation (27) by subtracting a factor $\sim 2.2 \exp(-t/\tau_{\text{dep}})$ such that

$$A'_{\text{tot}} \simeq -0.1 \quad \text{or} \quad A'_{\text{tot}} \simeq -2.1 \quad (33)$$

at $t = 0$ for co-orbiting and counter-orbiting IMC respectively. Following the discussion in the previous section, these values imply that, at least initially, the co-orbiting IMC has the possibility of exciting large e_{\star} than a counter-orbiting IMC (based on the magnitude of $e_{\star, \text{limit}}$ in Eq. 29 for these two cases). However, after a few τ_{dep} , the gas disk's contribution diminishes whereas the bulge potential does not change (see Figure 2). The values of A'_{tot} reduce to those in Equation (27) so that the secular perturbation by the counter-orbiting IMC can lead to large asymptotic e_{\star} . This adjustment is adiabatic in the limit $\tau_{\text{dep}} \gtrsim \tau_{\text{ecc}}$ (Nagasawa et al. 2003).

The above estimate is made for one particular value of a_{\star} (or equivalently α). In Equation (25), the contribution of the gas disk potential on the stars is proportional to $\alpha^{-1} \exp(-t/\tau_{\text{dep}})$. During the depletion of the gas disk, the significance of this term can be maintained at a smaller distance from the SMBH (see Figure 2). For a co-orbiting IMC, this inward propagation of the high-eccentricity-excitation region is referred

to as the sweeping secular resonance. Similarly, for a counter-orbiting IMC, the high-eccentricity excitation region sweeps outward. This property contrasts with the contribution from the Galactic bulge's potential which does not evolve with time.

Figure 1 is a schematic illustration of the physical process associated with the excitation of the disk stars due to the sweeping secular resonance of a co-orbiting IMC. Within a few pc from Sgr A*, SMBH's point-mass gravitational potential dominates the stellar orbits. Due to the IMC's secular perturbation, the stars' longitude of periastron liberates with eccentricity modulation as the angular momentum is exchanged between the IMC's and stellar orbits. The liberation period and amplitude are function of a_{IMC} , e_{IMC} , and a_{\star} (Eq. 24). Although the contribution from the Galactic disk and halo also leads to the precession of the stellar orbits, their effects are negligible within 1 pc from the SMBH. In contrast, the gravitational perturbation from the Galactic bulge and/or a compact geometrically thin gaseous disk leads to a pronounced precession of the longitude of periastron for both the IMC and the stars with eccentric orbits. With modest gravitationally-stable Σ distribution, the IMC and stellar precession rate are comparable to the liberation frequency it induces on the nearby stars. At some a_{\star} 's where these two frequencies resonate with each other, a finite angle of misalignment η is maintained between the longitudes of periastron of the IMC and the stars. This asymmetry leads to angular momentum transfer from the stars to the IMC and the excitation of e_{\star} .

The IMC's disk-induced precession frequency decreases during the depletion of the disk gas. The location of the secular resonance also propagates away from a_{IMC} . While the rate of eccentricity excitation does not depend on the disk depletion timescale, the asymptotic magnitude of e_{\star} does, in the limit $\tau_{\text{dep}} < \tau_{\text{ecc}}$. After the disk gas is severely depleted, the secular resonance sweeps through an extended region of the disk. We suggest this process is an efficient and robust eccentricity-excitation mechanism for a large fraction of stars that emerged out of the gaseous disk.

3.8. IMC with inclined orbit, Galactic disk, and halo

In the analysis in §3.6 and §3.7, we neglect contributions from the Galactic disk and halo because their contribution to the precession of IMC and stars in the inner parsec is negligibly small compared with those due to the IMC, Galactic bulge, and gaseous disk. In our numerical simulations, the validity of this approximation is verified. We also leave out, in the analytic study, the general possibility of an IMC with an inclined orbit rel-

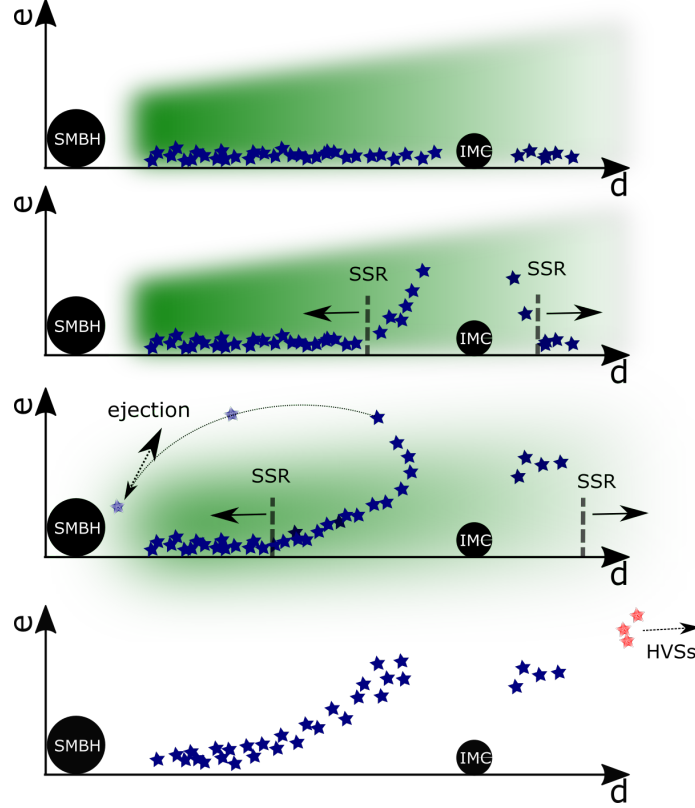


Figure 1. A schematic of the effects of the sweeping secular resonance (SSR) on the surrounding disk stars. The GC SMBH and an IMC are labeled with black dots, while blue stars represent the clockwise disk stars. The green shading represents a depleted gas disk, and its color dilutes with the decrease of the gas surface density. In the bottom panel, some hyper-velocity stars (HVSs) are shown with red stars. Their properties are studied in detail in paper II of this series.

ative to that of the stellar disk. A full 3D analysis introduces some additional degrees of freedom and dependent variables, including the inclination i and longitude of ascending node Ω . Although it is straightforward to follow the approach in celestial mechanics (Murray & Dermott 2000), it requires the presentation of lengthy algebra. For presentation purposes, we reserve the treatment of inclined orbits to our numerical simulations in the next section.

4. ECCENTRICITY EXCITATION BY SWEEPING SECULAR RESONANCE

The analysis in the previous section highlights the dominant effects of secular perturbation and sweeping secular resonance. We adopt several approximations to simplify the analytic treatment in the limit of small to modest e_* . The full effects can be calculated through the numerical integration of the Newtonian equation of motion with all or partial components of the contributing potentials, including the relativistic correction. Based on these numerical simulations, we show here how the IMC's secular perturbation may lead to the large eccentricity of CWSs. In paper II, we show that this process

may also lead to the ejection of some hyper-velocity stars (HVSs).

4.1. IMC's secular perturbation on a typical star

We first illustrate, with models NGD and CCW-NGD, the influence of IMC's secular perturbation on the disk stars in the absence of a gaseous disk. These models are identical to cases we have analyzed analytically in §3.6. With $a_{\text{IMC}} = 0.35$ pc and $e_{\text{IMC}} = 0.3$, the IMC gravitationally scatter many nearby stars. Their eccentricities quickly increase due to close encounters. Over time, the eccentricities of more distant stars are also excited by IMC's secular perturbation. In the previous section, we attribute this physical effect as the cause of CWSs' high eccentricity.

In order to compare with our analytic results (in §3.6 and §3.7), we follow the evolution of a representative star which had an initial $a_* = 0.15$ pc and $e_* = 0$. In the absence of a gaseous disk, the evolution of $\eta (\equiv \varpi_* - \varpi_{\text{IMC}})$ and $\xi (\equiv e_*/e_{\text{IMC}})$ in models NGD and CCW-NGD (for a co and counter orbiting IMC respectively) are plotted in the right panels of Figure 3. The discussion below Equation 28 is verified by the results of model NGD which show the evolution of η towards a critical value η_{crit}

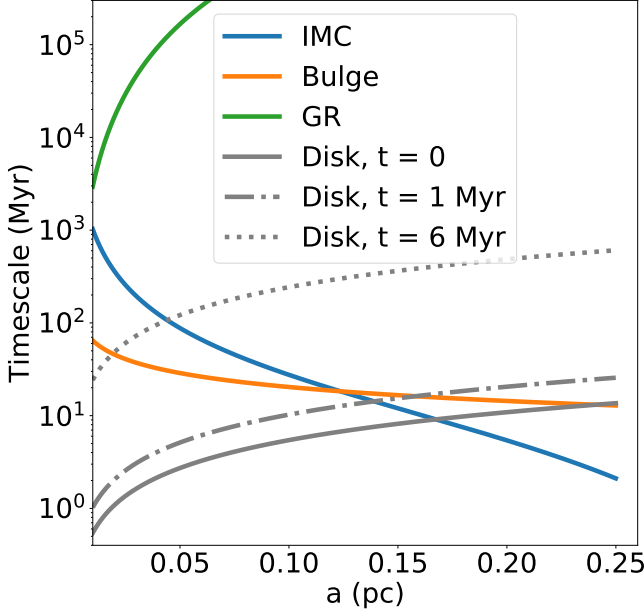


Figure 2. The precession timescale of one disk star as a function of its initial semi-major axis. The precession timescale is computed with different components, including the GR effect (solid green line), the secular perturbation of an IMC which is initially located at 0.35 pc with eccentricity equal to 0.3 (solid blue line), and the influence of gaseous disk with $\Sigma_0 = 600 \text{ g cm}^{-2}$, $\tau_{\text{dep}} = 1.58 \text{ Myr}$ at various stages (grey lines).

which is slightly larger than $-\pi/2$ in the limit of small e_* . Also in agreement with Equation 29, e_* makes a transition from monotonically growth to liberation over a limited range of η in model NGD. The range of ξ oscillates around limiting value ($e_{*,\text{limit}} \sim 0.1$ or equivalently $\xi_{\text{limit}} \sim 0.5$) on a time scale comparable to τ_{ecc} (Equation 30).

The results in model CCW-NGD show a slower monotonic growth of e_* (equivalent ξ). The difference in the eccentricity excitation time scale between models NGD and CCW-NGD is due to the difference in their magnitude of A'_{tot} (Eq. 27). As we have indicated in §3.6, model CCW-NGD is expected to produce a larger $e_{*,\text{limit}}$ than model NGD. If the calculation has continued beyond 6.3 Myr, this star would be ejected as its e_* becomes larger than unity.

4.2. Sweeping secular resonance due to gas depletion

The fiducial and CCW models (left panels of Figure 3) for a co and counter orbiting IMC embedded in an evolving gaseous disk with the stars are equivalent to the cases we have analyzed analytically in §3.7. The above discussion suggests that the gaseous disk's contribution to the gravitational field modifies the precession rate of both

IMC and the stars. In both models, the initial value of $A'_{\text{tot}} < 0$ (Eq. 33) such that their η_{crit} is slightly smaller than $-\pi/2$ in the limit of small e_* (Eq. 28). During the depletion of the disk, A'_{tot} increases to positive values so that η_{crit} becomes larger than $-\pi/2$ in both models. In the fiducial model, the star makes a transition from monotonic growth to circulation in which η varies between $-\pi$ and π . The value of e_* oscillates around a medium value which is larger than that in model NGD. Had the simulation continued beyond 6.3 Myr, the circulation cycle would be completed.

For the counter-orbiting IMC (model CCW), the initial surface density of the disk produces more negative values of A'_{tot} . Consequently the evolution of η_{crit} across $-\pi/2$ is delayed. At the end of the simulation, the propagation of the secular resonance promotes e_* to attain a larger value in model CCW than in model CCW-NGD. The magnitude of e_* continues to increase. Had the simulation continued beyond 6.3 Myr, this star would escape from SMBH's gravitational confine.

4.3. Statistical evolution of disk stars

The simulation of one representative star in the previous subsection is generalized to stars with a range of initial a_* . Although their eccentricity is excited, most of the disk stars with $a_* \lesssim 0.2 \text{ pc}$ in the NGD model, have asymptotic $e_* \lesssim 0.1$ (green dots in Figure 4), consistent with our estimate for $e_{*,\text{limit}}$ for the co-orbiting IMC (Eq. 29). These stars' modest liberation amplitudes limit their asymptotic e_* to be smaller than that observed.

The effect of sweeping secular resonance is noticeable in the fiducial model (yellow dots in Figure 4). At the end of the simulation, stars in the fiducial model generally attain larger e_* than those in the NGD model. As we have indicated in §3.7, for a co-orbiting IMC, sweeping secular resonance is required to excite the eccentricity of disk stars to the observed values.

For a counter-rotating IMC, the presence of the disk slows down the propagation of the secular resonance. The delayed eccentricity excitation in model CCW (with gaseous disk) to CCW-NGD (without gaseous disk) is contrasted by the yellow versus green dots in the left panel of Figure 5. At $t \gg \tau_{\text{dep}}$, the precession of IMC and stars in model CCW reduces to that in the CCW-NGD model. For the counter-orbiting IMC, stars acquire large eccentricities with or without the gaseous disk.

We also compare the SOFT and the fiducial model in the right panel of Figure 5, and find that whether the IMC is a point-mass like IMBH or a compact stellar cluster, it can produce comparable orbital excitation for

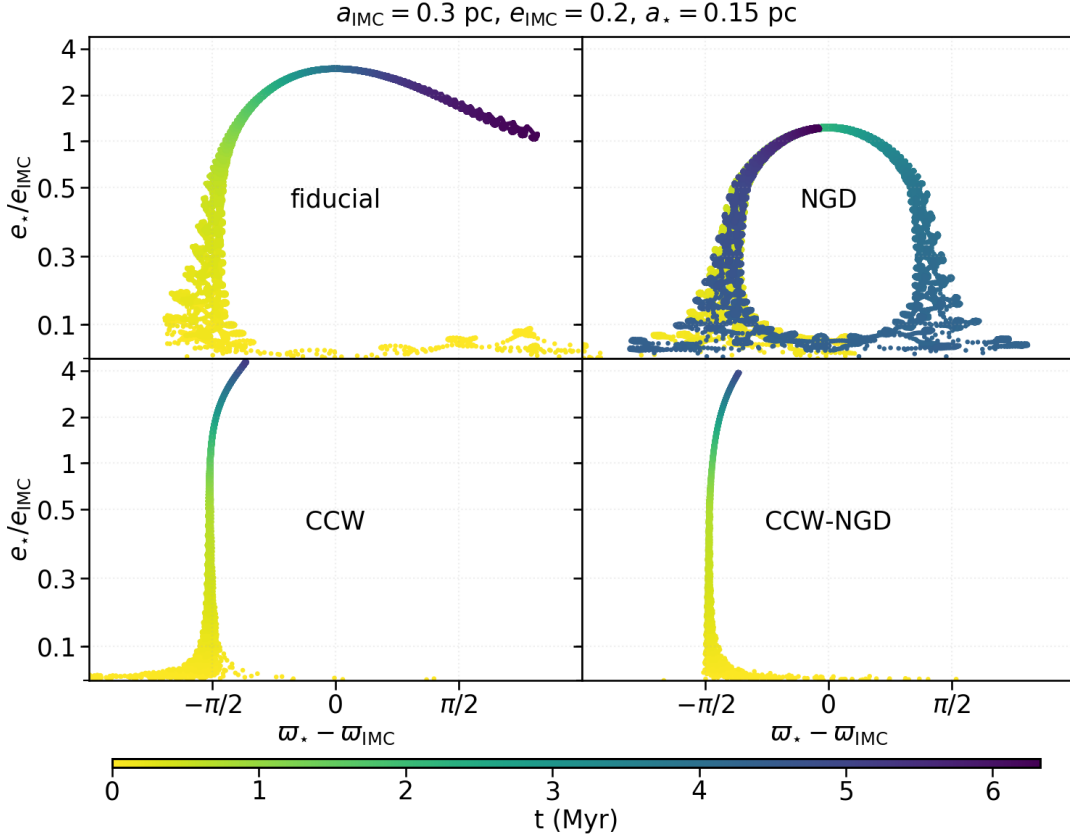


Figure 3. The representative orbital evolution track in the (ξ, η) -diagram. We trace the disk stars in the fiducial model, NGD model, CCW model, and CCW-NGD model. In the top panels, two models represent a co-orbiting IMC; In the bottom panels, they show a counter-orbiting IMC. In all models, these disk stars were initially on a circular orbit at 0.15 pc, while the IMC is orbiting with semi-major axes around 0.3 pc and eccentricity equal to 0.2. The color labels the time evolution, we trace from 0 Myr to 6.3 Myr.

these residual disk stars. However, an equal mass IMBH and a softening stellar cluster have the different capacity in stimulating high-velocity escapees, like HVSs. We intend to discuss related efficiency in paper II of this series.

4.4. Gaseous disk's mass and depletion timescale

For comparison, we simulated two versions of the fiducial model with the same M_{IMC} , a_{IMC} , and e_{IMC} . In these two models, the gaseous disks are assumed to have a) $\Sigma_0 = 600 \text{ g cm}^{-2}$ and $\tau_{\text{dep}} = 3.16 \text{ Myr}$ and b) $\Sigma_0 = 800 \text{ g cm}^{-2}$ and $\tau_{\text{dep}} = 1.58 \text{ Myr}$ (see yellow dots in the right and left panels, respectively, of Figure 4). The results of both models show that, within a few τ_{dep} , e_* is excited to $\gtrsim 0.3$ for most of the stars with $0.1 \text{ pc} \leq a_* \leq 0.4 \text{ pc}$. These values are comparable to those observed (see §4.5). These large eccentricities not only exceed those in model NCD, but they are extended over much wider radial distances from the SMBH. This outcome is due to the extensive region swept by IMC's secular resonance during the depletion of the gas disk,

as shown quantitatively in Equations (24) and (25) and quantitatively discussed in § 3.7.

For illustration purposes, we assume a hypothetical Σ distribution in our numerical models. The two chosen values of Σ_0 provide two different starting locations for IMC's secular resonance (Eq. 21). The magnitude of τ_{dep} determines the sweeping speed of IMC's secular resonances (Eq. 25). Protracted sweep (with larger τ_{dep}) prolongs the duration of angular momentum exchange and enhances the magnitude of excited eccentricity. Similar asymptotic values and distribution of e_* are excited by a range of combined Σ_0 and τ_{dep} values. Due to this degeneracy, we cannot constrain from the observed e_* distribution, the gas disk structural, and evolutionary parameters to some unique values. Nevertheless, these results also show that eccentricity excitation by sweeping secular resonance is generic and robust.

4.5. IMC's eccentricity and semi-major axis

The observed e_* distribution can be used to provide some constraints on a_{IMC} and e_{IMC} . In Figure 6, we

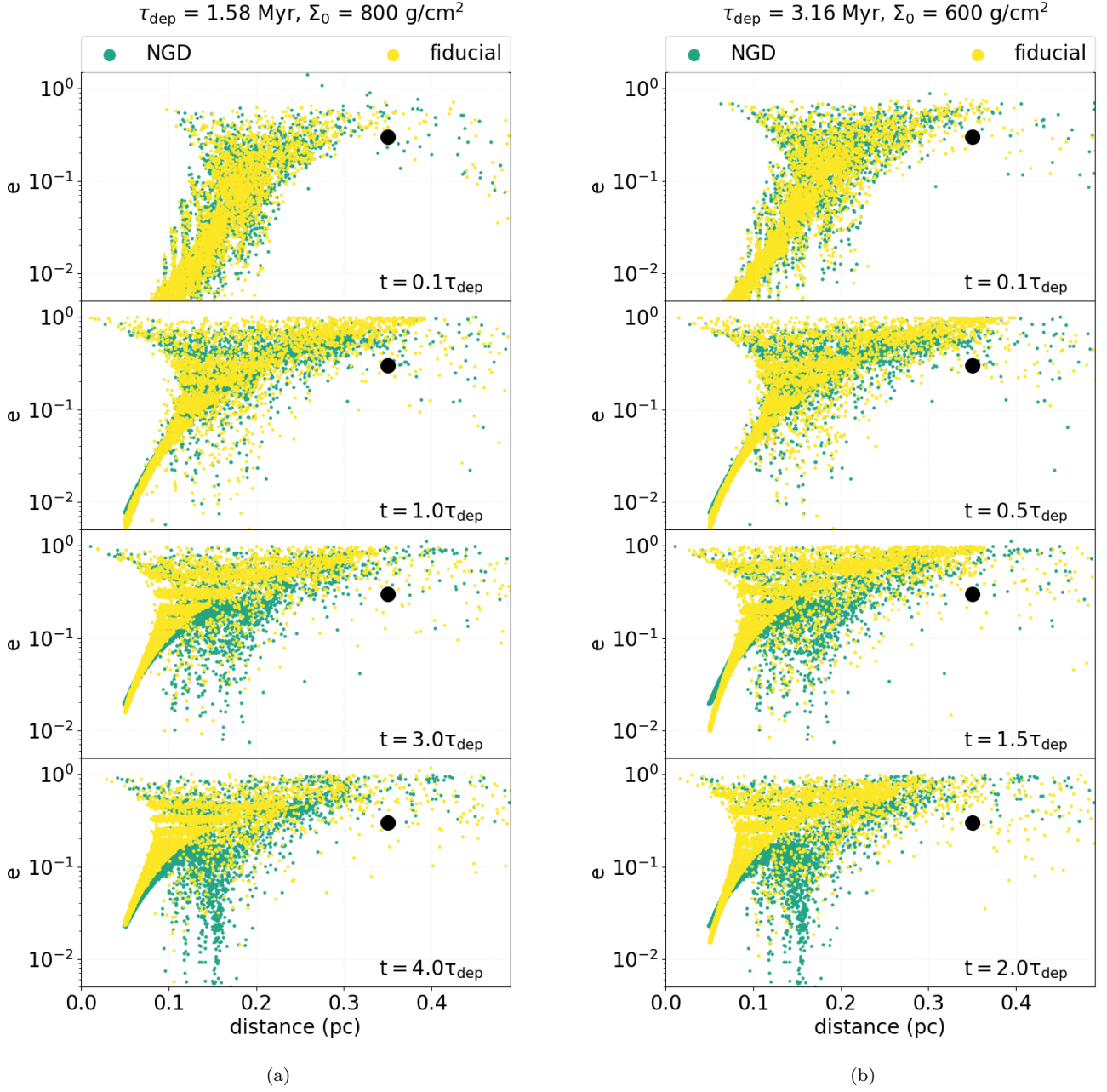


Figure 4. The effect of the sweeping secular resonance on the eccentricity excitation of disk stars. The simulated results of the fiducial model and NGD model are represented with yellow and green dots, respectively. The black dot is a potential IMC located at 0.35 pc distance to Sgr A * with an eccentricity of 0.3. Disk stars are uniformly distributed around 0.05 – 0.5 pc, except the region $a_{\text{in}} - a_{\text{out}}$. The left panels (a) represent the fiducial model with gas disk $\tau_{\text{dep}} = 1.58$ Myr and $\Sigma_0 = 800$ g/cm 2 , the right panels (b) represent the result of gas disk with $\tau_{\text{dep}} = 3.16$ Myr and $\Sigma_0 = 600$ g/cm 2 .

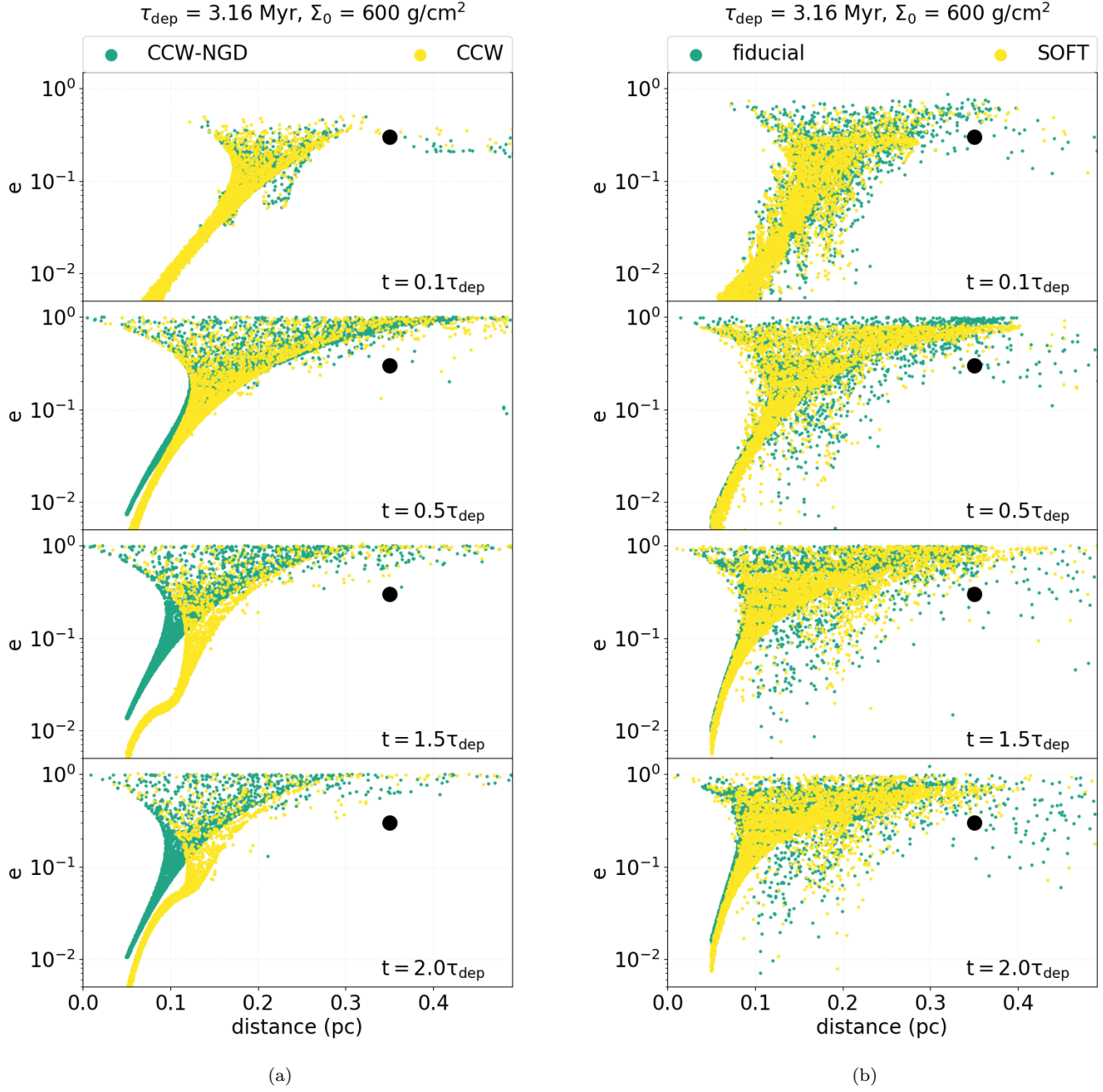


Figure 5. Same as Figure 4, but compare the fiducial model, SOFT model, CCW model, and CCW-NGD model. The left panels (a) represent the CCW model and CCW-NGD model. The right panels (b) represent the result of the fiducial model and SOFT model.

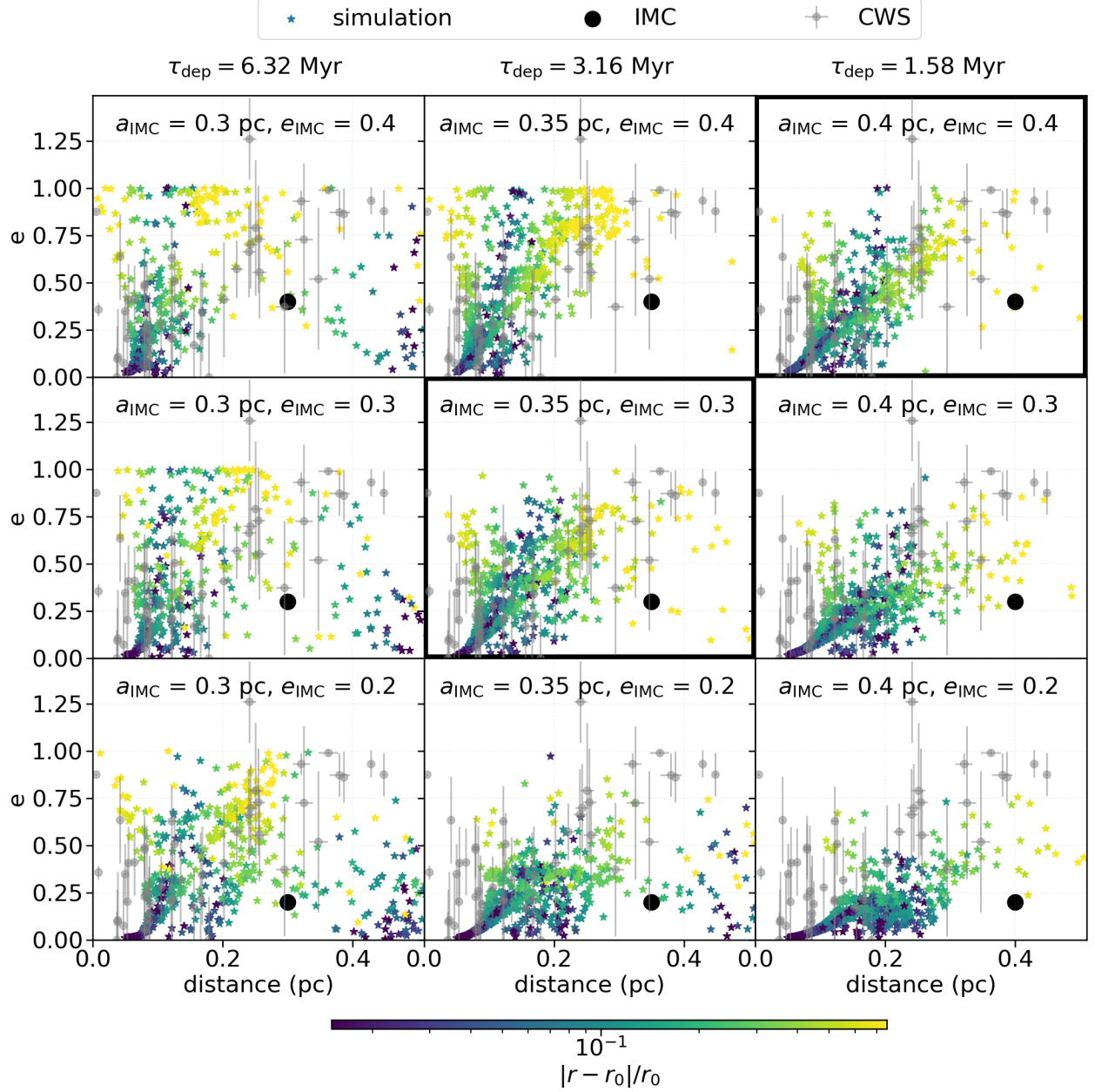


Figure 6. Eccentricity of clockwise disk stars as a function of their distance from the SMBH. The filled grey dots with error bars represent the observed CWSs as given by [Paumard et al. \(2006\)](#). The black dot depicts the possible orbital parameters ($a_{\text{IMC}}, e_{\text{IMC}}$) of an IMC. In the left, middle, and right columns, we adopt $a_{\text{IMC}} = 0.3$ pc with $\tau_{\text{dep}} = 6.32$ Myr, $a_{\text{IMC}} = 0.35$ pc with $\tau_{\text{dep}} = 3.16$ Myr, and $a_{\text{IMC}} = 0.4$ pc with $\tau_{\text{dep}} = 1.58$ Myr, respectively. In the top, middle, and bottom rows, we choose $e_{\text{IMC}} = 0.4, 0.3$, and 0.2 respectively. The filled stars show the e_* and a_* of the disk stars at 6 Myr. Colors label the fractional change in the disk stars' distance from the SMBH.

compare the orbital distribution of 1000 disk stars under the influence of an co-orbiting IMC's secular perturbation. In the fiducial models, we choose for IMC a mass $M_{\text{IMC}} = 10^4 M_{\odot}$ with various values of a_{IMC} ($= 0.3, 0.35, 0.4$ pc) and e_{IMC} ($= 0.2, 0.3, 0.4$) in the same orbital plane as the gaseous disk and the stars' initial orbital plane.

The disk stars are set initially with zero e_* and random a_* distribution between $0.05 - 0.5$ pc uniformly. For the purpose of highlighting the influence of sweeping secular resonance, stars initially in the close-encounter-with-the-IMC zone (between $a_{\text{in}} - a_{\text{out}}$) are excluded.

The observed a_* and e_* are plotted as grey dots in Figure 6. Up to ($\sim 80\%$) CWSs stars are located between $0.05 - 0.5$ pc and the high e_* (> 0.5) stars are

mostly located between 0.2 pc and 0.5 pc. Unless IMC has $e_{\text{IMC}} \sim 0.2 - 0.4$ and $a_{\text{IMC}} \sim 0.3 - 0.4$ pc, it is difficult to excite the eccentricity of disk stars to such high eccentricities. These numerical results are consistent with our analytic calculation in § 3.7.

All simulations are carried out over ~ 6 Myr with $\Sigma_0 = 600 \text{ g cm}^{-2}$. In order for IMC's secular resonance to sweep through most of regions with $a_* = 0.05 - 0.5$ pc for all the cases, we choose $\tau_{\text{dep}} = 6.32, 3.16$, and 1.58 Myr for $a_{\text{IMC}} = 0.3, 0.35$ and 0.4 pc respectively.

The results of these parameter study show two sets of preferred models which match the observational data: 1) $a_{\text{IMC}} = 0.35$ pc with $e_{\text{IMC}} = 0.3$, and 2) $a_{\text{IMC}} = 0.4$ pc with $e_{\text{IMC}} = 0.4$ (see Figure 6). In models with small $a_{\text{IMC}} (\leq 0.3 \text{ pc})$, the eccentricity excitation for $a_* \geq a_{\text{IMC}}$ is below ($\leq 0.2 - 0.5$) the observed e_* especially for the disk stars around $0.4 - 0.5$ pc. Similarly, in models with large $a_{\text{IMC}} (\geq 0.4 \text{ pc})$ and small $e_{\text{IMC}} (\leq 0.3)$, the eccentricity excitation for $a_* < a_{\text{IMC}}$ is mostly below the observed e_* especially for the disk stars around $0.1 - 0.2$ pc. (The probability of observing an IBH or dense stellar cluster with $a_{\text{IMC}} > 0.4$ pc and $e_{\text{IMC}} > 0.4$ at the current projected separation of 0.13 pc from the Sgr A* is relatively low). For $a_{\text{IMC}} \sim 0.35 - 0.4$ pc, modest $e_{\text{IMC}} (\sim 0.3 - 0.4)$, IMC is able to excite the eccentricity of the disk stars with an extended a_* ($\sim 0.05 - 0.5$ pc) to the observed values after a few Myr.

Similar constraints can also be obtained for a counter orbiting IMC. Since the initial gravitational potential in model CCW-NGD (and the asymptotic configuration in model CCW) already produce small A'_{tot} and large $e_{*,\text{limit}}$ (Eqs. 27 and 29), a more extended range of suitable a_{IMC} and e_{IMC} can lead to large asymptotic e_* .

4.6. IMC with an inclined orbit

We also carry out two series of simulations with an inclined IMC orbit, relative to the initial stars' (or gaseous disk) orbital plane by $i_0 = 30^\circ$ and 60° . In celestial mechanics, secular interaction between planets with inclined orbits leads to modulations in their inclination and eccentricity which are correlated through the approximate conservation of the Delaunay momentum $H_K = \sqrt{1 - e^2} \cos i$ (Murray & Dermott 2000). The inclination in this expression refers to that relative to an invariant plane. This conservative relationship is also applicable to analogous stellar systems (Naoz 2016). With sufficiently large mutual inclination, i , it is possible for the precession frequencies of periastron and ascending node to enter into a Lidov-Kozai resonance such that nearly parabolic eccentricity can be excited with a corresponding change in i (Lidov 1962; Kozai 1962; Innanen et al. 1997). Accordingly, even if starting with a

low-inclination configuration, the orbit of an inner disk star can still be excited to high values. If stars which undergo close encounters with the SMBH, it is possible for their orbits to flip from prograde to retrograde orientation due to the chaotic perturbation of such an eccentric IMC, as discussed as in the context of the eccentric Kozai-Lidov mechanism (Li et al. 2014b,a; Naoz 2016; Hansen & Naoz 2020). With the contribution of the Galactic bulge and the gaseous disk to the potential, the precession rates in the present context are modified from those associated with classical celestial mechanics. It also enlarges the amplitude of variation of the Delaunay momentum during a secular cycle.

In the top two rows of Figure (7), we plot the instantaneous radial distribution of e_* at the end of the simulation for models I30-NGD, I30, I60-NDG, and I60. Although the results in model NGD show that e_* is excited with $i_0 = 0$, a comparison between models NGD, I30-NGD, and I60-NGD indicates that a larger i_0 can enhance the oscillation amplitude in both e_* and i_* . However, a fraction of stars attains nearly parabolic e_* with large changes in i_* from the weakly perturbed stars.

In models I30 and I60 with gaseous disks, we assume the IMC cannot open a gap. Consequently, its precession due to the disk potential is in the same direction as the stars. The longitudinal precession rates of both periastron and ascending node evolve during the depletion of the disk. The amplitudes of e_* and i_* modulation are enhanced for stars with $a_* \gtrsim 0.2$ pc and suppressed for those with $a_* \lesssim 0.13$ pc, especially in model I60. The frequency of stars with highly eccentric and inclined orbits is increased by the perturbation of a highly inclined IMC. This diversity may account for the dispersion in the inclination of the young stars around Sgr A*.

In all the models we have considered so far, we assume the angular momentum vector of the gaseous disk (and that of the stars initially) is parallel to that of the Galactic disk. In the last row of Figure (7), we introduce model I60-IS60-NGD and I60-IS60. In these models, the stellar disk is initially 60° inclined to the Galactic disk (Table 2). Since the scale length for the Galactic disk is much larger than a_* , we do not expect any significant difference between models I60-IS60-NGD and I60-NGD (as well as between models I60-IS60 and I60) as shown in Figure (7). This agreement justifies the neglect of the Galactic disk and halo in the analytic calculation in §3.

5. SUMMARY & DISCUSSION

There is a population of very young and massive stars within the central 0.5 pc of the Galaxy. Many of them orbit clockwise around the SMBH on the same plane. These CWS's, especially those with semi-major axis

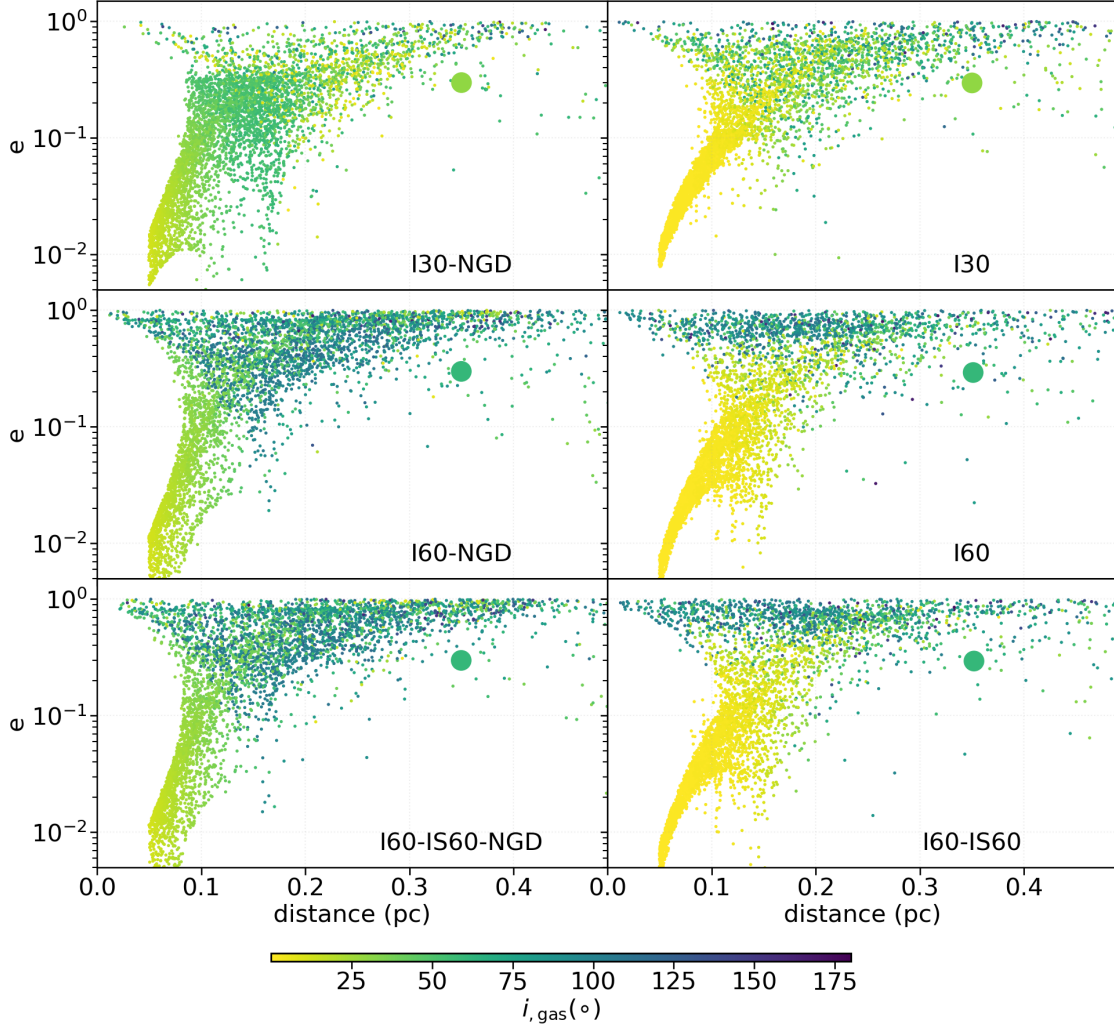


Figure 7. The eccentricity distribution of simulated stars around 6 Myr as a function of distance to the GC in the I30, I30-NGD, I60, I60-NGD, I60-IS60 and I60-IS60-NGD models. Colors label the inclination of disk stars (and IMC). i_{gas} refers to the mutual inclination between the orbits of the disk star (or IMC) and the gas disk. For these NGD models, it refers to the inclination of the disk stars (or IMC) relative to the disk stars’ initial orbital plane. The dot size labels the mass of disk stars and IMC.

$\sim 0.2 - 0.5$ pc, are observed to have large eccentricities relative to the SMBH ($e_{\star} \gtrsim 0.5$, see Figure 6). If they were formed in a nearly Keplerian disk with modest or negligible eccentricities, there would not be adequate time for the eccentricity of these massive stars to be excited, by their intrinsic dynamical relaxation process (Lightman & Shapiro 1977; Rauch & Tremaine 1996; Merritt 2013), to the observed values within their expected life span.

In this paper, we mainly focus on the possibility of a companion to the SMBH as the culprit of eccentricity excitation for the CWSs. We suggest a potential candidate, IRS 13E, which has a projected separation of 0.13 pc from Sgr A*. It has an estimated mass $\sim 10^4 M_{\odot}$ and somewhat uncertain orbital motion around the SMBH in the counter-clock direction. There have been sugges-

tions that it may be an IMBH or a compact stellar cluster. We refer this satellite perturber as an intermediate-mass companion, IMC. Since we are interested in its secular perturbation over a wide range of distances (a fraction of a pc), our analysis applies regardless whether it is an IMBH or a compact stellar cluster with a comparable mass.

We consider a range of semi-major axis ($a_{\text{IMC}} = 0.3 - 0.4$ pc) and eccentricity ($e_{\text{IMC}} = 0.2 - 0.4$) for the IMC. In order to circumvent the large observational uncertainty in its orbit, we consider both co-orbiting and counter-orbiting IMC which revolves around the SMBH either in the same or opposite direction as the CWSs. In paper II, we also examine the possibility of an IMC with inclined orbits relative to the CWSs.

We show there are several stages of stars' dynamical evolution. We assume the CWSs emerged in their natal disk with negligible initial eccentricity. Under the IMC's secular perturbation, their relative longitude of periastron η (with respect to that of the IMC) rapidly evolve to some quasi finite (non zero) values, initially slightly larger than $-\pi/2$. In this secular resonant state, the CWSs' precession is nearly synchronized with that of the IMC. Under the IMC's perturbation, CWSs' eccentricity e_* increases monotonically as their η increases toward 0 with a secular growth rate $\sim e_{\text{IMC}} n_{\text{IMC}} M_{\text{IMC}} / (4M_{\text{SMBH}})$. When e_* reaches an asymptotic limit $e_{*,\text{limit}}$, the stars exit their secular resonances with the IMC as the evolution of their η transforms from a protracted shift of quasi-equilibrium values to liberation within a limited range or circulates over 2π . During these secular cycles, the stars' eccentricity is modulated by the exchange of angular momentum between them and the IMC. If the potential of all the perturbing components remains constant, there would not be any additional systematic eccentricity evolution beyond $e_{*,\text{limit}}$ other than the modulation associated with liberation and circulation.

Our analysis shows that the eccentricity growth limit ($e_{*,\text{limit}}$) depends on the delicate balance between IMC and CWSs' precession frequencies. Both of these frequencies are partially determined by the IMC's and stars' relative direction of motion around the SMBH, the stationary mass ratios between the Galactic bulge, SMBH, and IMC. They also depend on the stars' semi-major axis (a_*), the ratio of CWSs' and IMC's eccentricity (ξ), and the evolving mass of the gas disk ($M_D \exp(-t/\tau_{\text{dep}})$). In the absence of an evolving gaseous disk, η makes a transition from the monotonic, slow shift of quasi-equilibrium to liberation or circulation with relative small $e_{*,\text{limit}}$ for a co-orbiting IMC. But, under the secular perturbation of a counter-orbiting IMC, the transition occurs for many stars, in the $0.2 - 0.5$ pc region, with much larger $e_{*,\text{limit}} (\gtrsim 0.5)$.

The youthfulness and the coplanar orbits of the CWSs suggest that they have emerged from a gaseous disk. Here, we assume an initial mass for the disk and its exponential depletion on a timescale of a few Myr. We speculate that this disk may be the reservoir of the Fermi bubble without specifying how it was launched. While the disk had a mass comparable to that of the IMC, its contribution to the gravitational potential significantly modified the stars' and IMC's precession rates from those due to their mutual secular interaction and the Galactic bulge potential. In this limit, e_* 's transition from monotonic growth to liberation or circulation

occurs with relative large $e_{*,\text{limit}}$ for a co-orbiting IMC and with modest $e_{*,\text{limit}}$ for a counter-orbiting IMC.

Since there is no sign of a gaseous disk today, it must have depleted after the formation of the CWSs. During the depletion of the gaseous disk, its influence on the IMC's and stars' precession wanes. This transformation extensively reduces/enlarges the high- $e_{*,\text{limit}}$ domain for a co-orbiting / counter-orbiting IMC respectively. We refer to this evolving landscape as the sweeping secular resonance. We carry out several series of systematic numerical simulations to demonstrate that the sweeping secular resonance can facilitate the potential excitation of e_* to the observed values ($\gtrsim 0.5 - 0.7$) of CWSs or the hyperbolic orbits of HVSSs. This sweeping secular resonance process is effective for both a co-orbiting and counter-orbiting IMC. But, without a gaseous disk, there would be no sweeping secular resonance, and the precession of a co-orbiting IMC alone would not ensure the excitation of adequately large e_* .

Based on this scenario, we compare the results of the numerical simulation with the observed eccentricity distribution of the CWSs to constrain the IMC's orbital semi-major axis to be in the range of $0.3 - 0.4$ pc which is somewhat larger than IRS 13E's projected separation from Sgr A* as suggested by the X-ray morphology of its surrounding region (Wang et al. 2020). We also find that for a co-orbiting IMC, the effectiveness of this process requires the depletion timescale (τ_{dep}) to be comparable to or larger than a fraction of the liberation timescale. Since a counter-orbiting IMC can excite high $e_{*,\text{limit}}$ without a disk, this condition is not required. Our numerical simulations also demonstrate that since its secular perturbation is applied through distant torque rather than short-range close encounters, the perturbing companion (i.e., IRS 13E) can be an IMBH or a compact bound stellar cluster with the same mass.

Our analysis highlights the sensitive dependence of CWSs' eccentricity on the IMC's mass and orbit. Yet the physical nature and integrity of our suggested candidate, IRS 13E, remain uncertain and controversial. Future observational determination of these parameters will be useful to constrain this model. Other poorly known quantities are the mass and depletion timescale of the hypothetical gaseous disk. A complementary model for the origin of the Fermi bubble may provide insights into the origin and evolution of the CWSs. In paper II of this series, we will also study the population of HVSSs in great detail.

In the work presented here, we assume a stable orbit of an eccentric IMC throughout the work. However, the dynamical friction by the surrounding stars leads to an orbital decay of the IMC in central regions of the

Galaxy, and the final decay inside the central parsec occurs within ~ 15 Myr (Just et al. 2011). Theoretically, the orbital migration of the IMC induces additional secular resonance sweeping through the central parsec, in analogy to the effect of a depleting gaseous disk. This effect has been studied in the solar system context (Agnor & Lin 2012). Also, we do not include binary configurations in this work. However, the existence of a binary population may influence the kinematic measurements, as discussed in Naoz et al. (2018). And the survival of any close binaries with hyper-velocity can provide a discriminate test between our model and the Hill’s mechanism. We will address these issues in the near future.

ACKNOWLEDGMENTS

Simulations in this paper made use of the REBOUND code which is publicly available at [REBOUND](https://github.com/mwalton/rebound) website. We thank Tuan Do, Stefan Gillessen, Mark Morris, and Hangci Du for useful conversation. This work is partly supported by the National Key Research and Development Program of China (No. 2018YFA0404501 to SM), by the National Science Foundation of China (Grant No. 11821303, 11761131004 and 11761141012 to SM) and by the China Postdoctoral Science Foundation (Grant No. 2017M610865 to XCZ).

Software: REBOUND (Rein & Liu 2012; Rein et al. 2019)

REFERENCES

- Agnor, C. B., & Lin, D. N. C. 2012, *ApJ*, 745, 143, doi: [10.1088/0004-637X/745/2/143](https://doi.org/10.1088/0004-637X/745/2/143)
- Alexander, R. D., Begelman, M. C., & Armitage, P. J. 2007, *ApJ*, 654, 907, doi: [10.1086/509709](https://doi.org/10.1086/509709)
- Artymowicz, P., Lin, D. N. C., & Wampler, E. J. 1993, *ApJ*, 409, 592, doi: [10.1086/172690](https://doi.org/10.1086/172690)
- Boehle, A., Ghez, A. M., Schödel, R., et al. 2016, *ApJ*, 830, 17, doi: [10.3847/0004-637X/830/1/17](https://doi.org/10.3847/0004-637X/830/1/17)
- Bub, M. W., & Petrovich, C. 2020, *ApJ*, 894, 15, doi: [10.3847/1538-4357/ab8461](https://doi.org/10.3847/1538-4357/ab8461)
- Do, T., Ghez, A. M., Morris, M. R., et al. 2009, *ApJ*, 703, 1323, doi: [10.1088/0004-637X/703/2/1323](https://doi.org/10.1088/0004-637X/703/2/1323)
- Do, T., Martinez, G. D., Yelda, S., et al. 2013, *ApJL*, 779, L6, doi: [10.1088/2041-8205/779/1/L6](https://doi.org/10.1088/2041-8205/779/1/L6)
- Freitag, M., Amaro-Seoane, P., & Kalogera, V. 2006, *ApJ*, 649, 91, doi: [10.1086/506193](https://doi.org/10.1086/506193)
- Generozov, A., & Madigan, A.-M. 2020, *ApJ*, 896, 137, doi: [10.3847/1538-4357/ab94bc](https://doi.org/10.3847/1538-4357/ab94bc)
- Genzel, R., Eckart, A., Ott, T., & Eisenhauer, F. 1997, *MNRAS*, 291, 219, doi: [10.1093/mnras/291.1.219](https://doi.org/10.1093/mnras/291.1.219)
- Genzel, R., Eisenhauer, F., & Gillessen, S. 2010, *Reviews of Modern Physics*, 82, 3121, doi: [10.1103/RevModPhys.82.3121](https://doi.org/10.1103/RevModPhys.82.3121)
- Genzel, R., Schödel, R., Ott, T., et al. 2003, *ApJ*, 594, 812, doi: [10.1086/377127](https://doi.org/10.1086/377127)
- Gerhard, O. 2001, *ApJL*, 546, L39, doi: [10.1086/318054](https://doi.org/10.1086/318054)
- Ghez, A. M., Becklin, E., Duchjne, G., et al. 2003a, *Astronomische Nachrichten Supplement*, 324, 527, doi: [10.1002/asna.200385103](https://doi.org/10.1002/asna.200385103)
- Ghez, A. M., Klein, B. L., Morris, M., & Becklin, E. E. 1998, *ApJ*, 509, 678, doi: [10.1086/306528](https://doi.org/10.1086/306528)
- Ghez, A. M., Duchêne, G., Matthews, K., et al. 2003b, *ApJL*, 586, L127, doi: [10.1086/374804](https://doi.org/10.1086/374804)
- Ghez, A. M., Salim, S., Weinberg, N. N., et al. 2008, *ApJ*, 689, 1044, doi: [10.1086/592738](https://doi.org/10.1086/592738)
- Gillessen, S., Eisenhauer, F., Fritz, T. K., et al. 2009, *ApJL*, 707, L114, doi: [10.1088/0004-637X/707/2/L114](https://doi.org/10.1088/0004-637X/707/2/L114)
- Gnedin, O. Y., Gould, A., Miralda-Escudé, J., & Zentner, A. R. 2005, *ApJ*, 634, 344, doi: [10.1086/496958](https://doi.org/10.1086/496958)
- Goodman, J. 2003, *MNRAS*, 339, 937, doi: [10.1046/j.1365-8711.2003.06241.x](https://doi.org/10.1046/j.1365-8711.2003.06241.x)
- Gürkan, M. A., & Rasio, F. A. 2005, *ApJ*, 628, 236, doi: [10.1086/430694](https://doi.org/10.1086/430694)
- Hansen, B. M. S., & Milosavljević, M. 2003, *ApJL*, 593, L77, doi: [10.1086/378182](https://doi.org/10.1086/378182)
- Hansen, B. M. S., & Naoz, S. 2020, *MNRAS*, doi: [10.1093/mnras/staa2602](https://doi.org/10.1093/mnras/staa2602)
- Hayashi, C., Nakazawa, K., & Nakagawa, Y. 1985, in *Protostars and Planets II*, ed. D. C. Black & M. S. Matthews, 1100–1153
- Hernquist, L. 1990, *ApJ*, 356, 359, doi: [10.1086/168845](https://doi.org/10.1086/168845)
- Innanen, K. A., Zheng, J. Q., Mikkola, S., & Valtonen, M. J. 1997, *AJ*, 113, 1915, doi: [10.1086/118405](https://doi.org/10.1086/118405)
- Just, A., Khan, F. M., Berczik, P., Ernst, A., & Spurzem, R. 2011, *MNRAS*, 411, 653, doi: [10.1111/j.1365-2966.2010.17711.x](https://doi.org/10.1111/j.1365-2966.2010.17711.x)
- Kenyon, S. J., Bromley, B. C., Geller, M. J., & Brown, W. R. 2008, *ApJ*, 680, 312, doi: [10.1086/587738](https://doi.org/10.1086/587738)

- Kidder, L. E. 1995, *PhRvD*, 52, 821, doi: [10.1103/PhysRevD.52.821](https://doi.org/10.1103/PhysRevD.52.821)
- Kim, S. S., Figer, D. F., & Morris, M. 2004, *ApJL*, 607, L123, doi: [10.1086/422032](https://doi.org/10.1086/422032)
- Kim, S. S., & Morris, M. 2003, *ApJ*, 597, 312, doi: [10.1086/378347](https://doi.org/10.1086/378347)
- Kozai, Y. 1962, *AJ*, 67, 591, doi: [10.1086/108790](https://doi.org/10.1086/108790)
- Krabbe, A., Genzel, R., Eckart, A., et al. 1995, *ApJL*, 447, L95, doi: [10.1086/309579](https://doi.org/10.1086/309579)
- Levin, Y., & Beloborodov, A. M. 2003, *ApJL*, 590, L33, doi: [10.1086/376675](https://doi.org/10.1086/376675)
- Levin, Y., Wu, A., & Thommes, E. 2005, *ApJ*, 635, 341, doi: [10.1086/497286](https://doi.org/10.1086/497286)
- Li, G., Naoz, S., Holman, M., & Loeb, A. 2014a, *ApJ*, 791, 86, doi: [10.1088/0004-637X/791/2/86](https://doi.org/10.1088/0004-637X/791/2/86)
- Li, G., Naoz, S., Kocsis, B., & Loeb, A. 2014b, *ApJ*, 785, 116, doi: [10.1088/0004-637X/785/2/116](https://doi.org/10.1088/0004-637X/785/2/116)
- Lidov, M. L. 1962, *Planet. Space Sci.*, 9, 719, doi: [10.1016/0032-0633\(62\)90129-0](https://doi.org/10.1016/0032-0633(62)90129-0)
- Lightman, A. P., & Shapiro, S. L. 1977, *ApJ*, 211, 244, doi: [10.1086/154925](https://doi.org/10.1086/154925)
- Löckmann, U., & Baumgardt, H. 2009, *MNRAS*, 394, 1841, doi: [10.1111/j.1365-2966.2009.14466.x](https://doi.org/10.1111/j.1365-2966.2009.14466.x)
- Lu, J. R., Ghez, A. M., Hornstein, S. D., et al. 2006, in *Journal of Physics Conference Series*, Vol. 54, *Journal of Physics Conference Series*, 279–287, doi: [10.1088/1742-6596/54/1/044](https://doi.org/10.1088/1742-6596/54/1/044)
- Lu, J. R., Ghez, A. M., Hornstein, S. D., et al. 2009, *ApJ*, 690, 1463, doi: [10.1088/0004-637X/690/2/1463](https://doi.org/10.1088/0004-637X/690/2/1463)
- Madigan, A.-M., Halle, A., Moody, M., et al. 2018, *ApJ*, 853, 141, doi: [10.3847/1538-4357/aaa714](https://doi.org/10.3847/1538-4357/aaa714)
- Madigan, A.-M., Hopman, C., & Levin, Y. 2011, *ApJ*, 738, 99, doi: [10.1088/0004-637X/738/1/99](https://doi.org/10.1088/0004-637X/738/1/99)
- Madigan, A.-M., Levin, Y., & Hopman, C. 2009, *ApJL*, 697, L44, doi: [10.1088/0004-637X/697/1/L44](https://doi.org/10.1088/0004-637X/697/1/L44)
- Madigan, A.-M., Pfuhl, O., Levin, Y., et al. 2014, in *IAU Symposium*, Vol. 303, *The Galactic Center: Feeding and Feedback in a Normal Galactic Nucleus*, ed. L. O. Sjouwerman, C. C. Lang, & J. Ott, 238–241, doi: [10.1017/S1743921314000659](https://doi.org/10.1017/S1743921314000659)
- Maillard, J. P., Paumard, T., Stolovy, S. R., & Rigaut, F. 2004, *A&A*, 423, 155, doi: [10.1051/0004-6361:20034147](https://doi.org/10.1051/0004-6361:20034147)
- Merritt, D. 2013, *Dynamics and Evolution of Galactic Nuclei*
- Murray, C. D., & Dermott, S. F. 2000, *Solar System Dynamics* (Cambridge University Press), doi: [10.1017/CBO9781139174817](https://doi.org/10.1017/CBO9781139174817)
- Nagasawa, M., Lin, D. N. C., & Ida, S. 2003, *ApJ*, 586, 1374, doi: [10.1086/367884](https://doi.org/10.1086/367884)
- Nagasawa, M., Lin, D. N. C., & Thommes, E. 2005, *ApJ*, 635, 578, doi: [10.1086/497386](https://doi.org/10.1086/497386)
- Naoz, S. 2016, *ARA&A*, 54, 441, doi: [10.1146/annurev-astro-081915-023315](https://doi.org/10.1146/annurev-astro-081915-023315)
- Naoz, S., Ghez, A. M., Hees, A., et al. 2018, *ApJL*, 853, L24, doi: [10.3847/2041-8213/aaa6bf](https://doi.org/10.3847/2041-8213/aaa6bf)
- Naoz, S., Will, C. M., Ramirez-Ruiz, E., et al. 2020, *ApJL*, 888, L8, doi: [10.3847/2041-8213/ab5e3b](https://doi.org/10.3847/2041-8213/ab5e3b)
- Nayakshin, S., Cuadra, J., & Springel, V. 2007, *MNRAS*, 379, 21, doi: [10.1111/j.1365-2966.2007.11938.x](https://doi.org/10.1111/j.1365-2966.2007.11938.x)
- Paumard, T., Genzel, R., Martins, F., et al. 2006, *ApJ*, 643, 1011, doi: [10.1086/503273](https://doi.org/10.1086/503273)
- Petrovich, C., & Antonini, F. 2017, *ApJ*, 846, 146, doi: [10.3847/1538-4357/aa8628](https://doi.org/10.3847/1538-4357/aa8628)
- Portegies Zwart, S. F., Makino, J., McMillan, S. L. W., & Hut, P. 2002, *ApJ*, 565, 265, doi: [10.1086/324141](https://doi.org/10.1086/324141)
- Rauch, K. P., & Tremaine, S. 1996, *NewA*, 1, 149, doi: [10.1016/S1384-1076\(96\)00012-7](https://doi.org/10.1016/S1384-1076(96)00012-7)
- Reid, M. J., & Brunthaler, A. 2004, *ApJ*, 616, 872, doi: [10.1086/424960](https://doi.org/10.1086/424960)
- Rein, H., & Liu, S. F. 2012, *A&A*, 537, A128, doi: [10.1051/0004-6361/201118085](https://doi.org/10.1051/0004-6361/201118085)
- Rein, H., Tamayo, D., & Brown, G. 2019, *MNRAS*, 489, 4632, doi: [10.1093/mnras/stz2503](https://doi.org/10.1093/mnras/stz2503)
- Rodriguez, C. L., Amaro-Seoane, P., Chatterjee, S., et al. 2018, *PhRvD*, 98, 123005, doi: [10.1103/PhysRevD.98.123005](https://doi.org/10.1103/PhysRevD.98.123005)
- Schödel, R., Eckart, A., Iserlohe, C., Genzel, R., & Ott, T. 2005, *ApJL*, 625, L111, doi: [10.1086/431307](https://doi.org/10.1086/431307)
- Schödel, R., Merritt, D., & Eckart, A. 2009, *A&A*, 502, 91, doi: [10.1051/0004-6361/200810922](https://doi.org/10.1051/0004-6361/200810922)
- Su, M., Slatyer, T. R., & Finkbeiner, D. P. 2010, *ApJ*, 724, 1044, doi: [10.1088/0004-637X/724/2/1044](https://doi.org/10.1088/0004-637X/724/2/1044)
- Tremaine, S. D. 1976, *ApJ*, 203, 345, doi: [10.1086/154085](https://doi.org/10.1086/154085)
- Tsuijboi, M., Kitamura, Y., Tsutsumi, T., et al. 2017, *ApJL*, 850, L5, doi: [10.3847/2041-8213/aa97d3](https://doi.org/10.3847/2041-8213/aa97d3)
- Wang, Q. D., Li, J., Russell, C. M. P., & Cuadra, J. 2020, *MNRAS*, 492, 2481, doi: [10.1093/mnras/stz3624](https://doi.org/10.1093/mnras/stz3624)
- Ward, W. R. 1981, *Icarus*, 47, 234, doi: [10.1016/0019-1035\(81\)90169-X](https://doi.org/10.1016/0019-1035(81)90169-X)
- Widrow, L. M., & Dubinski, J. 2005, *ApJ*, 631, 838, doi: [10.1086/432710](https://doi.org/10.1086/432710)
- Yu, Q., & Tremaine, S. 2003, *ApJ*, 599, 1129, doi: [10.1086/379546](https://doi.org/10.1086/379546)
- Zheng, X., Lin, D. N. C., & Kouwenhoven, M. B. N. 2017a, *ApJ*, 836, 207, doi: [10.3847/1538-4357/836/2/207](https://doi.org/10.3847/1538-4357/836/2/207)
- Zheng, X., Lin, D. N. C., Kouwenhoven, M. B. N., Mao, S., & Zhang, X. 2017b, *ApJ*, 849, 98, doi: [10.3847/1538-4357/aa8ef3](https://doi.org/10.3847/1538-4357/aa8ef3)

Zhu, Z., Li, Z., Ciurlo, A., et al. 2020, ApJ, 897, 135,
doi: [10.3847/1538-4357/ab980d](https://doi.org/10.3847/1538-4357/ab980d)